

Design, operation and optimization of an atomic absorption spectrometer with a constant temperature furnace
by Frederic Garland Dewalt

A thesis submitted in partial fulfillment of the requirements for the degree of DOCTOR OF PHILOSOPHY in Chemistry
Montana State University
© Copyright by Frederic Garland Dewalt (1982)

Abstract:
An examination has been made of problems associated with early constant temperature designs. This information is applied to producing continually better constant temperature furnaces.

A simple electronic system which corrects for both broad band absorption and broad band emission is presented.

Changing internal graphite part dimensions inside electrothermal atomizers results in changing the temperature profile of the absorption tubes which may alter sample signals. Effects of changing these parts in a constant temperature furnace is discussed. Effects of changing some other operational parameters such as argon flow and sample insertion rate are also discussed.

A temperature controlled annealing oven for glasswork is presented as an aid for preparation of analytical glassware.

Design, Operation and Optimization of an Atomic Absorption Spectrometer with a Constant Temperature Furnace

by

FREDERIC GARLAND DEWALT

A thesis submitted in partial fulfillment
of the requirements for the degree

of

DOCTOR OF PHILOSOPHY

in

Chemistry

Approved:

Chairperson, Graduate Committee

Head, Major Department

Graduate Dean

MONTANA STATE UNIVERSITY
Bozeman, Montana
May, 1982

ACKNOWLEDGEMENT

A very special thanks to Dr. Ray Woodriff for his warmth, understanding, advice, constant support and great enthusiasm for both science and off the road excursions. I am deeply indebted to Dr. John Amend for his assistance in designing and building electronic components. His help and guidance thoughout my academic career is much appreciated. I also wish to thank all the residents here in Gaines Hall for making my education a fruitful and generally enjoyable experience. A special thanks to Pat Gillis for her understanding and literary expertise.

TABLE OF CONTENTS

	Page
Vita	ii
Acknowledgement	iii
Table of Contents	iv
List of Tables	vii
List of Figures	viii
Abstract	xi
Chapter 1 - General Atomic Absorption	1
1.1 Brief Introduction	1
1.2 Fundamental Principles of Atomic Absorption Spectroscopy	1
1.3 General Spectrometer Design	2
1.3.1 Light Sources	2
1.3.2 Monochrometers	3
1.3.3 Detectors	3
1.3.4 Atomizers	4
1.3.4.1 Brief Introduction	4
1.3.4.2 Flames	4
1.3.4.3 Electrothermal Atomizers	5
Chapter 2 - Designs and Operation of Constant Temperature Furnaces	7
2.1 Introduction	7
2.2 History of Woodriff Furnace Design	8

Page

2.2.1 Introduction 8

2.2.2 Single Phase Furnaces 8

2.2.3 Three Phase Furnaces 19

2.2.4 Sample Introduction Systems 26

2.3 Operating Parameters 27

2.3.1 Atomizer Temperature 27

2.3.2 Argon Flow 29

2.3.3 Sample Preparation 29

2.3.4 Sensitivity 33

Chapter 3 - Supporting Electronics for the Constant Temperature Furnace 36

3.1 Introduction 36

3.2 A Stable Hollow-Cathode Power Supply 36

3.2.1 Introduction 36

3.2.2 Circuit Description 36

3.2.3 Applications 42

3.3 A Background Emission Correction System for Atomic Absorption Spectroscopy 46

3.3.1 Introduction 46

3.3.2 Circuit Description 50

3.3.3 Experimental Results and Discussion 57

3.3.4 Conclusion 66

Page

Chapter 4 - Optimization of the Constant Temperature Furnace . 68

4.1 Introduction 68

4.2 General Experimental 68

4.2.1 Electrical 68

4.2.2 Reagents and Materials 70

4.3 Experiments, Results and Discussion 70

4.3.1 Effects of Structural Changes on Temperature 70

4.3.2 Effects of Argon Flow and Sample Insertion Rate . . 76

4.3.3 Three Phase versus Single Phase Furnaces 86

Chapter 5 - Conclusions, Summary and Suggestions for Further Work 89

Appendix 92

References 100

LIST OF TABLES

Table		Page
1.	Sensitivity data for the Woodriff furnace	35
2.	Performance for the pulsed hollow-cathode light source .	45

LIST OF FIGURES

Figure		Page
1.	Cross-sectional view of the constant temperature furnace, model 2	10
2.	Cross-sectional view of the constant temperature furnace, model 4	12
3.	Cross-sectional view of the center sections of constant temperature furnace models 5 and 6	14
4.	Wiring diagram for single phase and three phase furnaces	17
5.	Temperature profiles for a single phase furnace, three phase furnace and simulated single phase furnace	18
6.	Simplified current flow diagram for three phase type heating	20
7.	Cross-sectional view of a three phase constant temperature furnace	22
8.	Cross-sectional views of graphite heater tube connectors	25
9.	Cross-sectional view of a newly proposed furnace	28
10.	Diagram of focusing system used on constant temperature furnaces	30
11.	Types of sample crucibles used in constant temperature furnaces	32
12.	Circuit diagram for the pulsed hollow-cathode power supply	38
13.	Diagram of the circuit used to measure current stability of the P.H.C.P.S.	43
14.	Circuit diagram of the crystal clock	44

Figure		Page
15.	Block diagram of an earlier atomic absorption system .	47
16.	Circuit diagram of the timing section of the BECS . . .	51
17.	Circuit diagram of the computation section of the BECS	52
18.	Diagram of the outputs of the timing section of the BECS	53
19.	Diagram of the outputs of the integrators in the computation section of the BECS	54
20.	Block diagram of the overall BECS system	58
21.	Circuit diagram for the input amplifier	60
22.	Circuit diagram for the voltage to frequency converter	61
23.	Plot of lamp intensity drifts and the BECS's ability to measure a constant simulated absorbance	63
24.	Circuit used to generate stable light signals	64
25.	Data showing the system's ability to correct for broad band absorption	67
26.	Circuit diagram of the sample insertion marker	69
27.	Effects of internal graphite part changes on temperature profiles in a three phase furnace	73
28.	Temperature versus Pb absorbance curves under varying conditions of Ar flow rate and sample pedestal condition	77
29.	Diagram of strip chart recorder tracings showing the effect of NaCl on Pb signals	81

Figure		Page
30.	Pb absorbance versus concentration curves under varying conditions of sample insertion rate and Ar flow	82
31.	Diagram of strip chart recorder tracings showing premature atomization for slowly inserted samples . . .	83
32.	Circuit diagram for the temperature controlled annealing oven	94

ABSTRACT

An examination has been made of problems associated with early constant temperature designs. This information is applied to producing continually better constant temperature furnaces.

A simple electronic system which corrects for both broad band absorption and broad band emission is presented.

Changing internal graphite part dimensions inside electrothermal atomizers results in changing the temperature profile of the absorption tubes which may alter sample signals. Effects of changing these parts in a constant temperature furnace is discussed. Effects of changing some other operational parameters such as argon flow and sample insertion rate are also discussed.

A temperature controlled annealing oven for glasswork is presented as an aid for preparation of analytical glassware.

CHAPTER 1

General Atomic Absorption

1.1 Brief Introduction

Atomic absorption spectroscopy has come a long way since Kirchhoff and Bunsen first established this type of light absorption in a series of papers published in the 1860's (1-4). Advantages of atomic absorption for chemical analysis were not fully recognized until the independent publications of Walsh (5) and of Alkemade and Milatz (6,7) appeared in 1955. Some of the first reported applications of this technique by Allan (8) and David (9) used an air-acetylene flame to determine magnesium and zinc in plants. After introduction of the nitrous oxide-acetylene flame by Willis (10) in 1965, rapid growth in atomic absorption methods occurred which replaced many classical chemical methods of analysis. Likewise, rapid growth in the development of atomic absorption spectrometer systems has occurred. Today atomic absorption spectrometers are fast and relatively inexpensive making atomic absorption analysis commonplace in many laboratories.

1.2 Fundamental Principles of Atomic Absorption Spectroscopy

All atomic absorption spectrometers contain four basic components used to measure the absorption of an atom cloud at a specific wavelength, i.e., a light source, an atomizer, a dispersion device

(monochromator) and a detector with some type of readout system. The spectrum of the element under study is emitted by the light source. The atom cloud, produced from a sample placed in the atomizer, absorbs a portion of the radiation coming from the light source. The portion of the radiation observed is selected by use of the dispersion device which allows a narrow band width of the spectrum to strike the detector. The detector "sees" an attenuation of the light coming from the light source when an absorbing sample is in the optical path, i.e., in the atomizer. This attenuation of light is governed by Lambert-Beers law

$$A = \log \frac{Io}{I} = abc$$

where there exists a linear relationship between the absorbance (A) and the concentration (c) of the element. Both the absorptivity (a) and the absorption path length (b) are constants.

1.3 General Spectrometer Design

1.3.1 Light Sources

Most atomic absorption spectrometers employ hollow cathode lamps (HCLs) for light sources. The cathode is a hollowed out cylinder constructed entirely or in part of the metal whose spectrum is to be produced. The anode and cathode are sealed in a glass envelope filled with either neon or argon. When an electrical potential is applied across the anode and cathode, a sputtering process occurs. The

spectrum of the cathode material is thus produced. Some of the more volatile elements make poor hollow cathode lamps. Eletrodeless discharge lamps (EDLs) are sometimes used for these elements. EDLs are made by sealing a small amount of the element or salt of the element inside a quartz bulb with an inert gas. Excitation of the element is accomplished by ionization of the inert gas with an external RF field. Both HCLs and EDLs usually have quartz end windows to emit radiation in the ultra violet region of the spectrum.

1.3.2 Monochrometers

Many types of monochromators have been designed and used utilizing prisms or gratings as dispersion devices. Great advances in grating manufacture in recent years have produced extremely good monochromators with no coma and no astigmatism capable of very narrow band widths. However, too narrow a band width can result in inaccurate background correction using continium lamp type correction as will be discussed in Chapter 3.

Atomic absorption light sources have simple spectra, unlike atomic emission where spectral emission lines are numerous, thus in most cases average quality monochromators can be used equally as well as the more expensive high resolution types.

1.3.3 Detectors

Photomultiplier tubes are the most often used detectors for atomic

absorption. Photodiode arrays have been used in multichannel detector systems (11), but these are less sensitive then photomultipliers in the UV region and have limited response linearity. Readouts for the photomultiplier signals have greatly advanced along with the recent advances made in the field of electronics. Early readouts consisted of simple transmittance and absorbance calibrated meters. Todays modern instruments store and process detector information with various data handling schemes, some using microprocessor control. These recent major advances in electronics have helped reduce errors associated with data handling far below errors orginating in other areas of the spectrometer.

1.3.4 Atomizers

1.3.4.1 Brief Introduction

Most errors involved with analysis by atomic absorption originate in the atomizer. Many of these errors are chemical in nature and atomizer design can greatly affect the analysis of real samples by altering the chemical reactions taking place inside the atomizer. There are two major classes of atomizers commonly used in atomic absorption analysis; flames and electrothermal atomizers.

1.3.4.2 Flames

Atomization by flames is the most commonly used technique for producing an atom cloud. The great appeal of this type of atomizer

stems from its simple and inexpensive design. Flame type atomizers can be operated by personnel with minimal training making it the choice for routine trace metal analysis by most laboratories. However, flames have a great many disadvantages. The disadvantages have been well documented (12-17) and have been discussed by Stone (18) and Lundberg (19). Even with all its disadvantages, flames will continue to be popular since many samples can successfully and inexpensively be analyzed with this method.

1.3.4.3 Electrothermal Atomizers

Most commerically available electrothermal atomizers are of the pulsed-heated type. These atomizers produce greater absolute sensitivities and correspondingly lower limits of detection than flame atomization. This is due to confining the atoms in a small volume within the optical path. These pulsed-heated type atomizers are very popular and are used in many laboratories for trace metal analysis. However, most of these atomizers suffer from various matrix interferences mainly due to the sample experiencing rapidly changing temperatures during atomization. An excellent review of the problems associated with these types of atomizers is given by Lawson (20). Success at eliminating matrix interferences from lead determinations in steel using a pulsed-heated type carbon rod atomizer was achieved by Lundberg and Frech (21). They eliminated matrix interferences by

introducing the samples after the atomizer reached it final temperature. Operation of an atomizer under isothermal conditions thus can greatly improve analysis. Although major manufacturers of commercial atomizers have yet to build and sell such an isothermal device for routine analyses, Woodriff has been using homemade constant temperature furnaces for about 15 years.

Woodriff's atomizer is relatively free from matrix interferences which plague many of the commercially available pulsed-heated electrothermal atomizers (22,23). This atomizer has several other important advantages which will be discussed in the following chapter. The main disadvantages stem from its complexity and expense. Advances in the design and understanding of the constant temperature furnace, as will be discussed in the following chapters, have helped to make it a more easily manipulated atomic absorption instrument for routine analysis. Hope remains, from work presented in this thesis, that commerical manufacturers of pulsed-heated electrothermal atomizers will take the initiative to develop and sell constant temperature atomizers for accurate direct analysis of samples with difficult matrices.

CHAPTER 2

Designs and Operation of Constant Temperature Furnaces

2.1 Introduction

Two different constant temperature furnaces were developed independently for use in Atomic Absorption. One type was developed by L'vov (17,24,25) in Russia. In L'vov's system, the atomizer and five or six samples on the end of carbon rods are placed in an evacuated chamber. Argon is introduced until the desired pressure (up to 8 or 9 atm.) is reached. Next, the atomization tube is heated to constant temperature. The carbon rod containing the dried sample is next inserted into a hole in the bottom side of the atomizer tube and is heated by auxiliary power atomizing the sample.

Woodriff (26) first reported his constant temperature furnace in 1966. The Woodriff furnace atomizer, with a much longer heater tube than L'vov's, operates at atmospheric pressure. The longer tube compensates for shorter analyte residence times at atmospheric pressure compared to L'vov's higher operating pressures. Operating the atomizer at atmospheric pressure allows direct introduction of samples from the outside without power interuption, depressurizing or re-loading sample rods as required by L'vov's design

once the limited number of samples contained inside the chamber have been atomized.

2.2 History of Woodriff Furnace Design

2.2.1 Introduction

The furnace design was constantly improved following its introduction in 1966 (26) through a total of ten different models. Each successive model provided new insights or improvements. With only a few exceptions (27), the internal resistive heating elements of the Woodriff furnace are made from graphite. The best graphite our research group uses for this purpose is Poco graphite (28) grade AFX-5Q. This is a very hard, easily machined graphite with low porosity. Insulation for these furnaces is generally made using 6 mm thick graphite felt from Union Carbide Corporation (29).

2.2.2 Single Phase Furnaces

The first furnace model (26,30) used a central graphite tube, 8 mm O.D. by 6 mm I.D., for the resistive heating element. This tube was surrounded by other concentric graphite tubes and graphite felt insulation, all housed inside a steel cylinder. Argon enters the furnace at a side tube connecting the center of the heater tube with the outside of the furnace. Samples are inserted and atomized on low conductivity rods pushed through the side tube until contact is made with the "hot" heater tube. Although good preliminary data was

gathered with this model, it had drawbacks. The heater tube was open to the air on the ends causing rapid deterioration. Inefficient cooling caused this model to become excessively hot, making handling difficult. Its rigid design did not allow for heater tube expansion causing frequent tube breakage.

The second model (Figure 1), first introduced by Woodriff and Ramelow in 1968 (31), solved the problem of tube breakage. Graphite plates mounted on spring loaded bolts held heater tube ends allowing for expansion as well as providing good electrical contact at high temperatures. Improved cooling was achieved by forcing water through copper tubing brazed to the housing of the furnace. Rapid deterioration of heater tube ends continued to plague this model due to back diffusion of oxygen into the atomizer.

Woodriff, et. al. (32,33) designed another model, which provided even more efficient cooling for easier handling. This third model used a metal, water cooled, spring loaded, electrical connector to hold the heater tube ends. This model also contained a massive "tee" connector connecting the side tube to the heater tube. The massive "tee" connector increased the heat capacity of the central part of the heater tube decreasing sample atomization time. These design changes, although they improved the operation of the furnace, also caused some

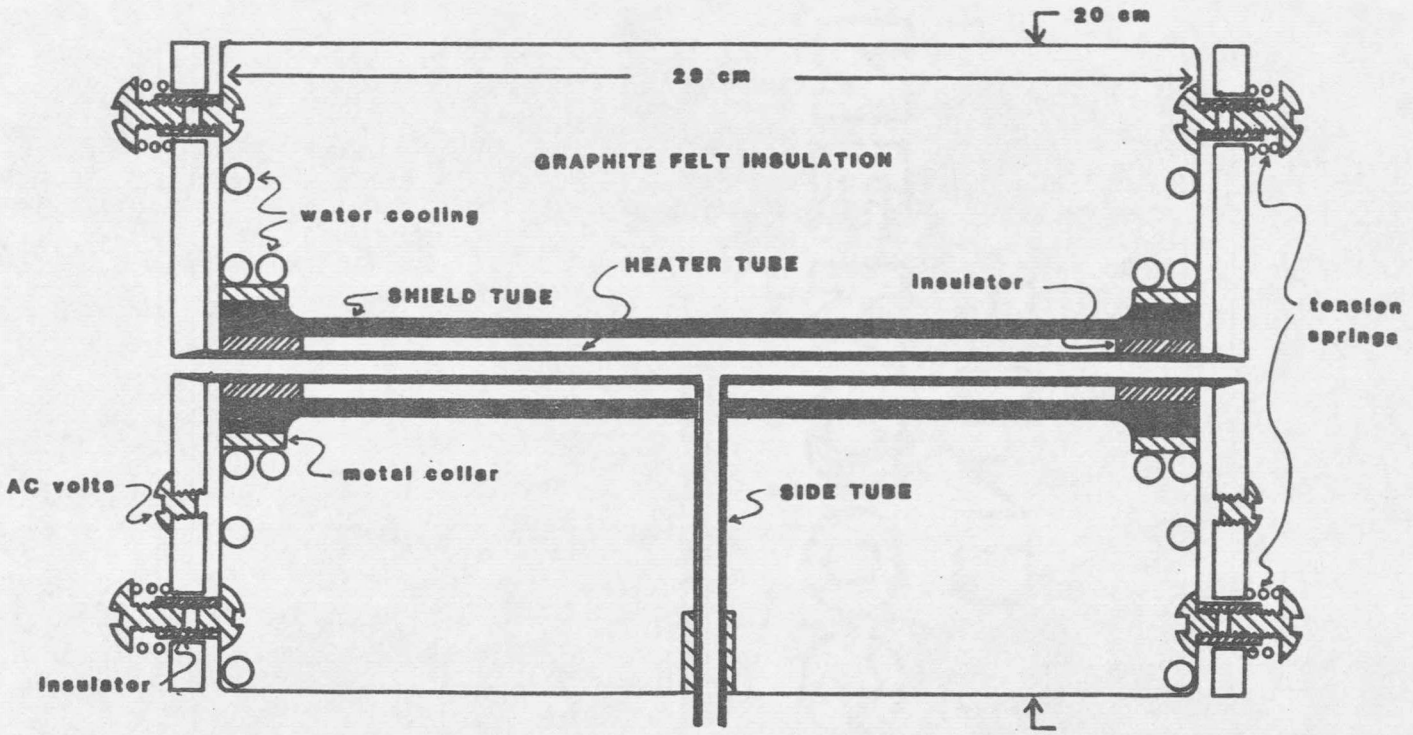


Figure 1. Cross-sectional view of constant temperature furnace, Model 2.

detrimental effects. More efficient cooling of the heater tube end connectors caused excessive cooling of the tube ends. Deposition of sample vapor on to the tube ends thus became a problem. A massive tee connector in the center gave a similar effect. A larger center has less resistance and thus a lower voltage drop than adjacent furnace parts. This including the larger surface area allowing increased radiative heat loss, results in a lower temperature. The side tube also contributes by conducting heat away from the center to the furnace housing. Thus a cold spot is produced at the point of sample introduction. Variation in heater tube temperature profile as a sample vapor travels down the tube might possibly lead to some matrix interferences. Analyte residence times can change if temperature gradients are large enough. The ultimate goal is to design a system with a uniform temperature profile down the heater tube. Such a system is extremely difficult to build while still providing proper cooling of the electrical connections as well as keeping the furnace itself cool enough for an operator to handle.

The fourth model (34,35) was the first design allowing the heater tube ends to be sealed inside the water cooled steel shell (see Figure 2). The tube ends were held with a spiral heater tube contact. This contact was constructed by coiling up copper tubing in a flat coil spiralling into the center to a graphite disk drilled to fit the heater

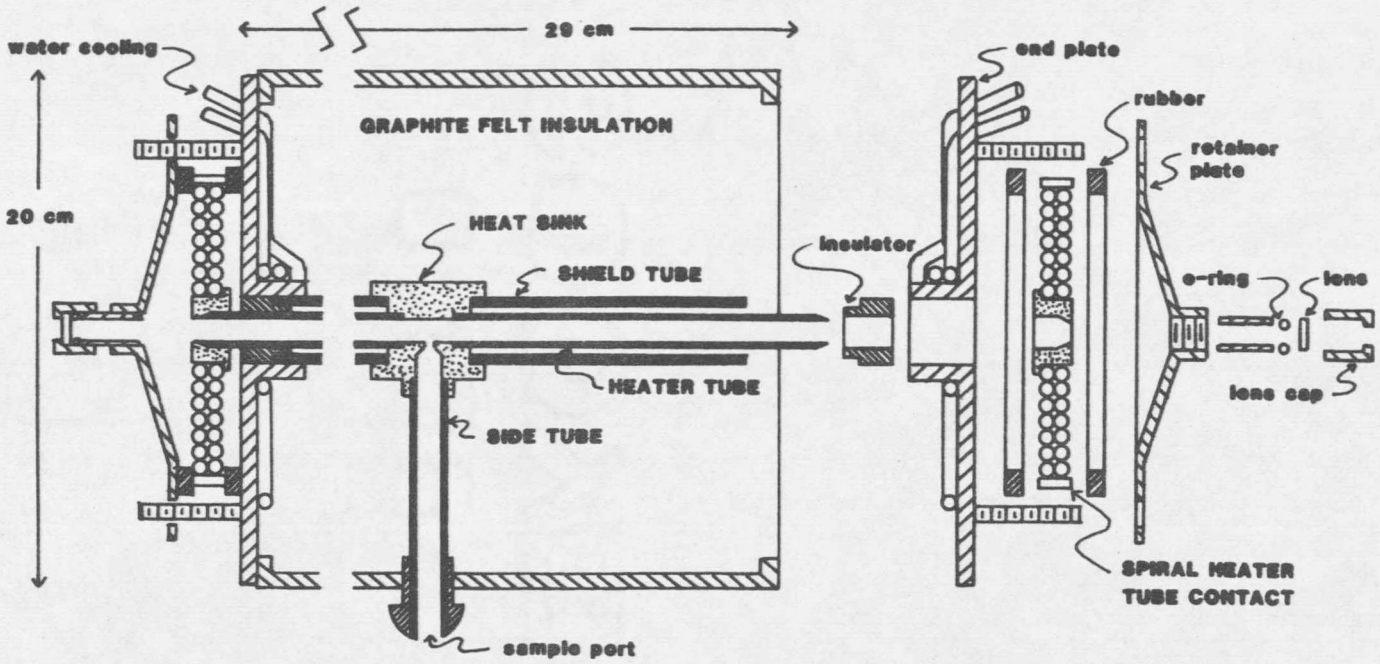
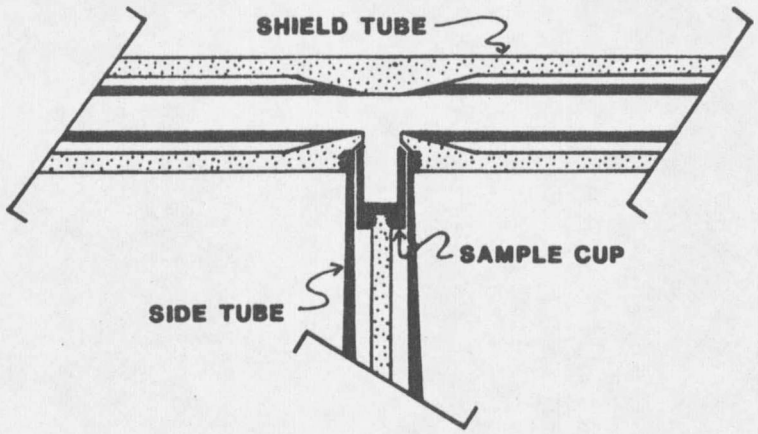


Figure 2. Cross-sectional view of constant temperature furnace, Model 4.

tube end. The copper tubing is then spiraled back out to the outside of the coil. This contact allowed for water cooling, electrical connection and was also springy enough to allow for graphite expansion. Its flat design allowed it to be squeezed between two plates and thus sealed on to a cylinder to form an airtight housing for the heater tube. Argon was introduced just inside the sample port at the end of the side tube. When the sample port is opened to insert a sample, argon flows out of the port washing oxygen off the sample. When the sample port is closed, argon flushes through the furnace and exits through a port made in each spiral heater tube contact. Both heater tube and shield tube in this model were made in two halves in order to simplify construction (shorter tubes are easier to drill from rod stock).

A number of studies (36-40) used the fifth model partially diagramed in Figure 3. It had two distinct differences from the previous design. The side tube wall, next to its connection with the shield tube, was made very thin, reducing heat conduction away from the center of the heater tube. Water cooling of the furnace housing was greatly improved by constructing it from a double jacketed stainless steel shell.

A single simple design change of the fifth model produced a new design with significant improvements over previous models. The sixth



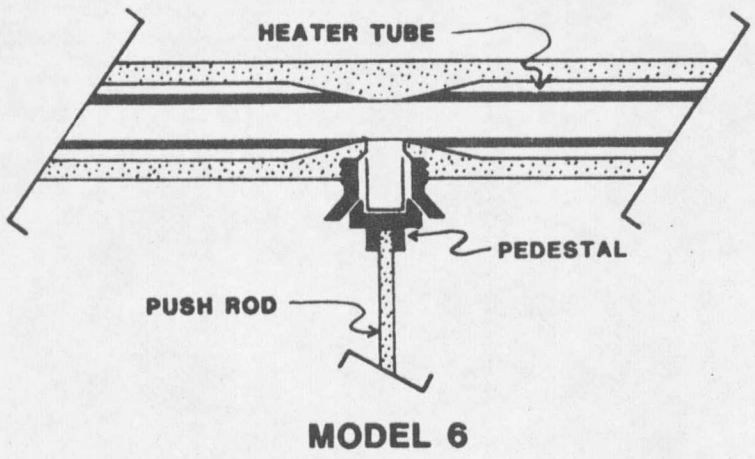


Figure 3. Cross-sectional view of center sections of constant temperature furnace, Models 5 and 6.

model was made by substituting a very small bell shaped entrance port for the side tube as indicated in Figure 3 (41). Existence of a side tube not only conducts heat away from the center of the heater tube, but can also cause contamination problems. As sample cups are inserted into the side tube, some of the sample material can transfer onto the side tube to be later re-transferred onto different sample cups. The result is sample loss in some cases and sample contamination in others. Removal of the side tube eliminated this problem (18). Unfortunately, however, removal of the side tube also eliminated the ability to direct nebulized samples into the heater tube (18,30,31,33-35). Previous to this model, sample introduction was accomplished by either nebulization or by sample placement in a graphite crucible. These graphite crucibles were manufactured with a threaded bottom for attachment to a thin graphite push rod. Upon insertion through the side tube, the rim of the crucible made a seal with a constriction at the top of the side tube. When using this technique with uncoated crucibles, it was found that individual crucibles consistently gave slightly higher or lower sensitivity, depending on the seal they make with the atomization chamber and on the rate of diffusion through their walls (42). This problem was solved by placing the crucible on a pedestal which makes the seal rather than the crucible rim. This method was subsequently used in all future designs. A number of successful studies were done

utilizing this sixth model (23,41-44). A smaller version of this model was also designed and used for easy placement into commercial spectrophotometers (45).

This stage of advancement in design of these furnaces marks the end of development of the single phase furnaces. The term single phase represents the type of electrical powering used to heat the heater (or absorption) tube. Single phase furnaces are typically heated by utilizing single phase 220 volt AC power. This voltage is first dropped across an autotransformer for power control, then run through a ten to one step down transformer before attachment to the heater tube ends (Figure 4).

Single phase furnaces all have the disadvantage of possessing an uneven heater tube temperature profile. The necessity of sample placement at the center of the heater tube causes a cooler temperature at that point which cannot be overcome by single phase heating. For example, in the sixth model the center temperature is typically 60-100°C lower than adjacent parts while heater tube end temperatures can be 600 to 1000°C lower (see Figure 5). The tube end temperatures can be raised considerably by suspending them on posts, but raising the cooler center temperature was solved only by switching to three phase type heating.

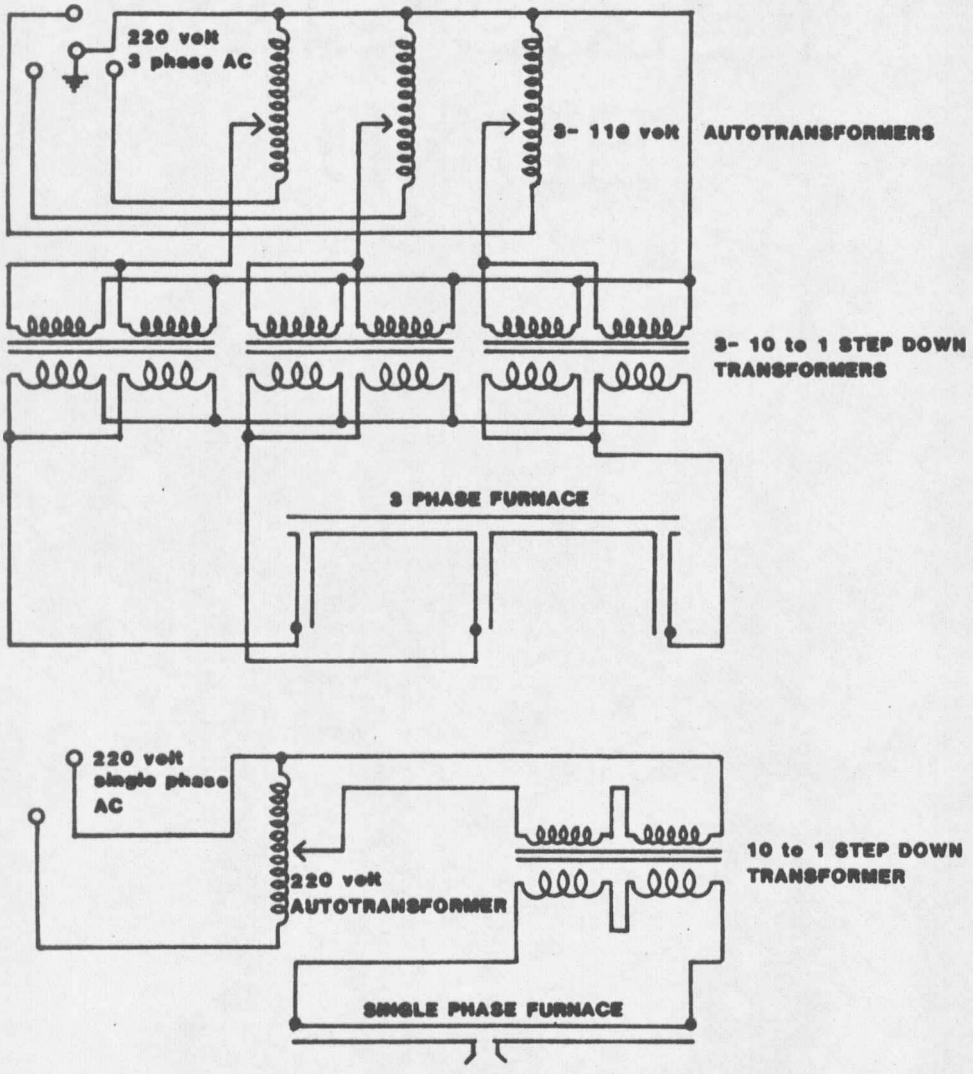


Figure 4. Wiring diagram for single phase and 3 phase furnaces.

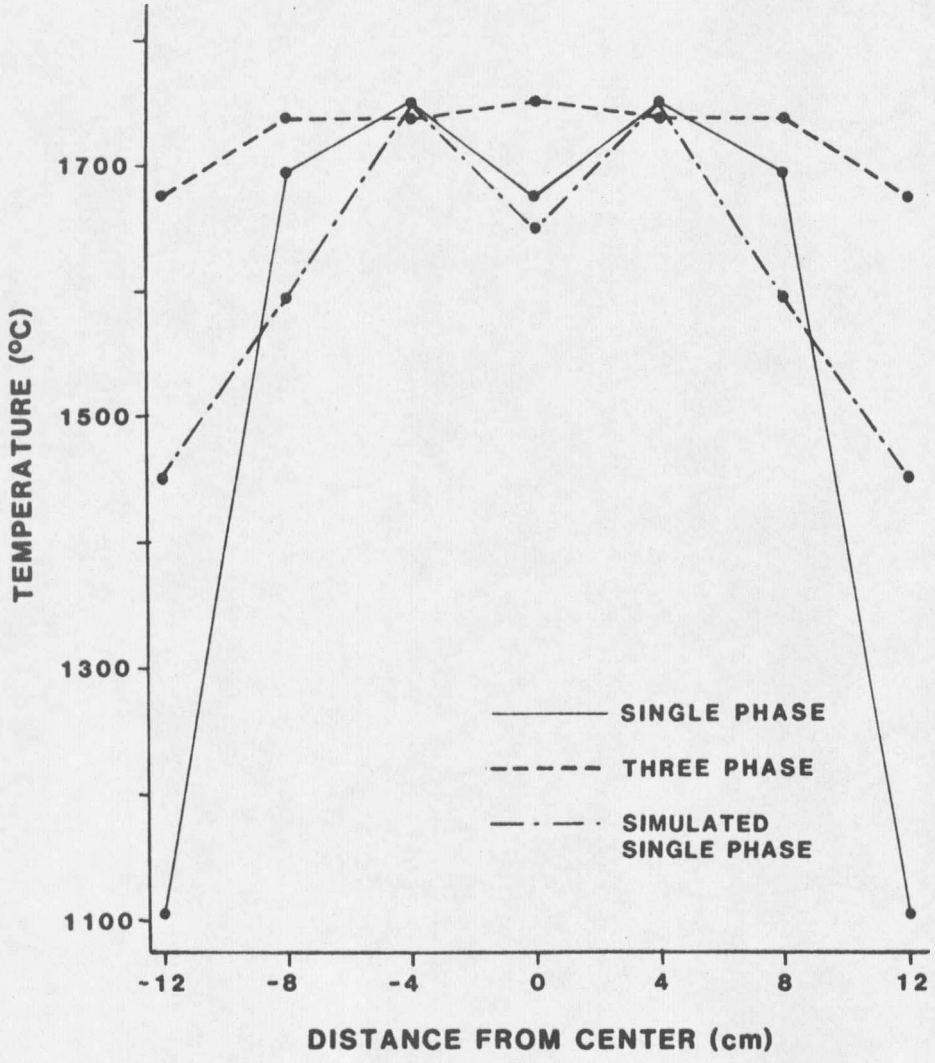


Figure 5. Temperature profiles of a single phase furnace (end held, Model 6), a three phase furnace (post held) and a simulated single phase profile inside a three phase furnace as discussed in Chapter 4.

2.2.3. Three phase furnaces

Three phase heating was first introduced by Woodriff (46) in 1976 and is subsequently used for powering all newer models (22, 47-53). Electrical hookup is accomplished by connecting each leg of the furnace (each side of the heater tube plus the side tube) to different phases of a 220 volt three phase AC power source by way of an autotransformer and step down transformer (Figure 4). The effect of such an arrangement can be easily understood by use of the simplified current flow diagram shown in Figure 6. When the left side of the heater tube (point 1) is at its most positive potential, the main current flow is from point 1 to both the right side of the heater tube (point 2) and the side tube (point 3). Likewise, later in time when the right side of the heater tube is at its most positive potential, the main current flow is to points 1 and 3. A similar situation occurs when the side tube is at its most positive potential. Considering only these three points in the complete three phase cycle, only four lines of current flow travel through each leg while six lines of current flow travel through the center "tee" connection. The result is that more current passes through the center than either of the three legs alone, causing the center to be the hottest part of the furnace. Marinkovic and Woodriff (49) showed that in order to minimize temperature decreases upon sample insertion, the tube connection should be made as massive as

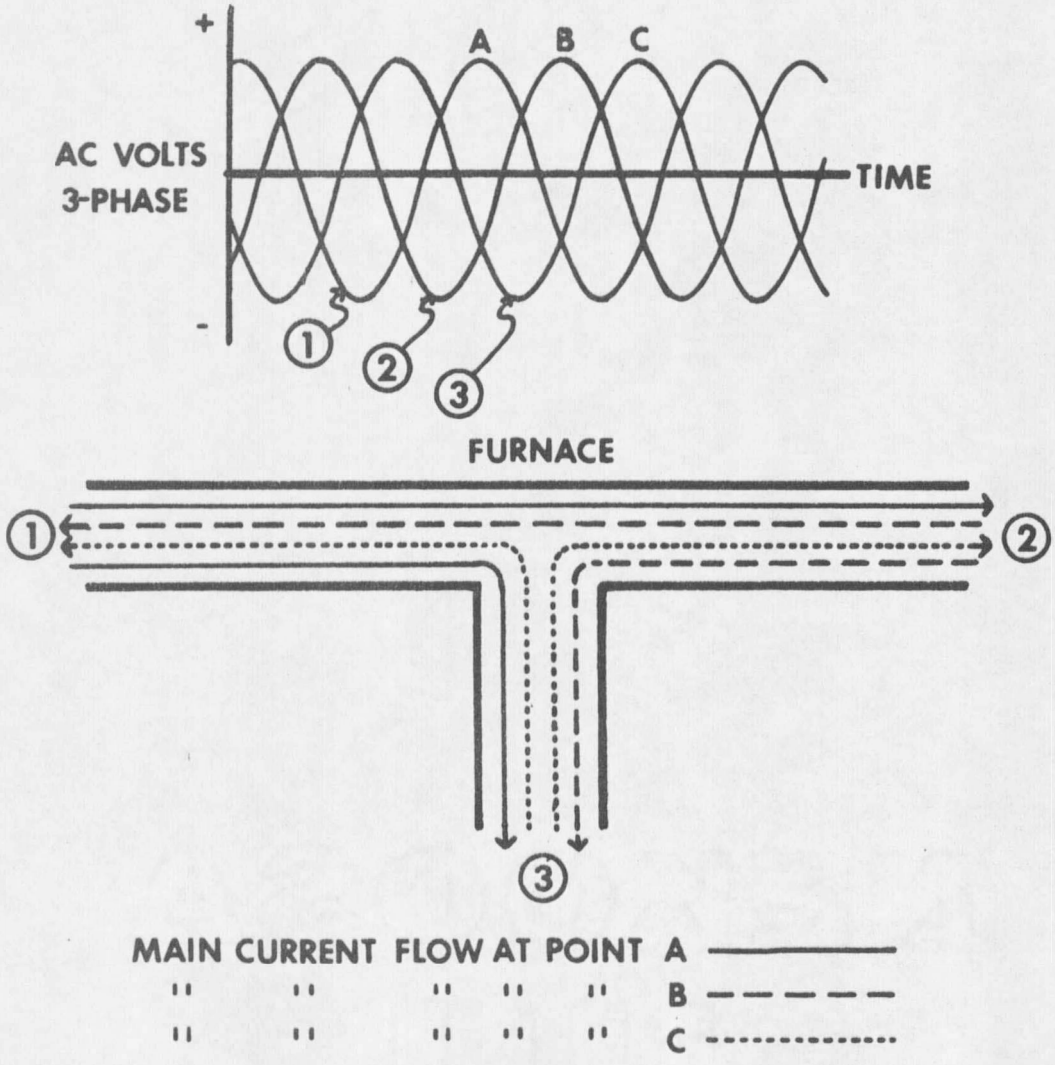


Figure 6. Simplified current flow diagram for 3 phase type heating in a constant temperature furnace.

possible. Since massive tube connections have less resistance than adjacent parts, more current flow through this connection is necessary to keep it from having a lower temperature than other parts of the tube. The much cooler heater tube end temperatures were raised in the newer three phase models by suspending the heater tube ends on graphite posts (50,53).

Near uniform temperatures can be achieved by utilizing the independent power control on each leg of a three phase furnace as shown in Figure 5.

An advanced three phase furnace is shown in Figure 7. Examination of its design will show some additional improvements over single phase models. All early single phase models possessed a guard or shield tube which surrounded the heater tube. The original purpose for this piece was to maintain optical stability, help insulate the heater tube, and keep graphite felt from contacting and thus shorting out the heater tube. This part was later found to be unnecessary. Good graphite felt insulation alone provided adequate insulating ability. This insulation can be easily cut and placed so that minimal contact with internal parts are made. If slippage of felt causing some heater tube contact does occur, the felt quickly burns back. This is probably due to its inability to maintain the high currents used to power the furnace. Optical stability of the heater tubes is maintained due to the side

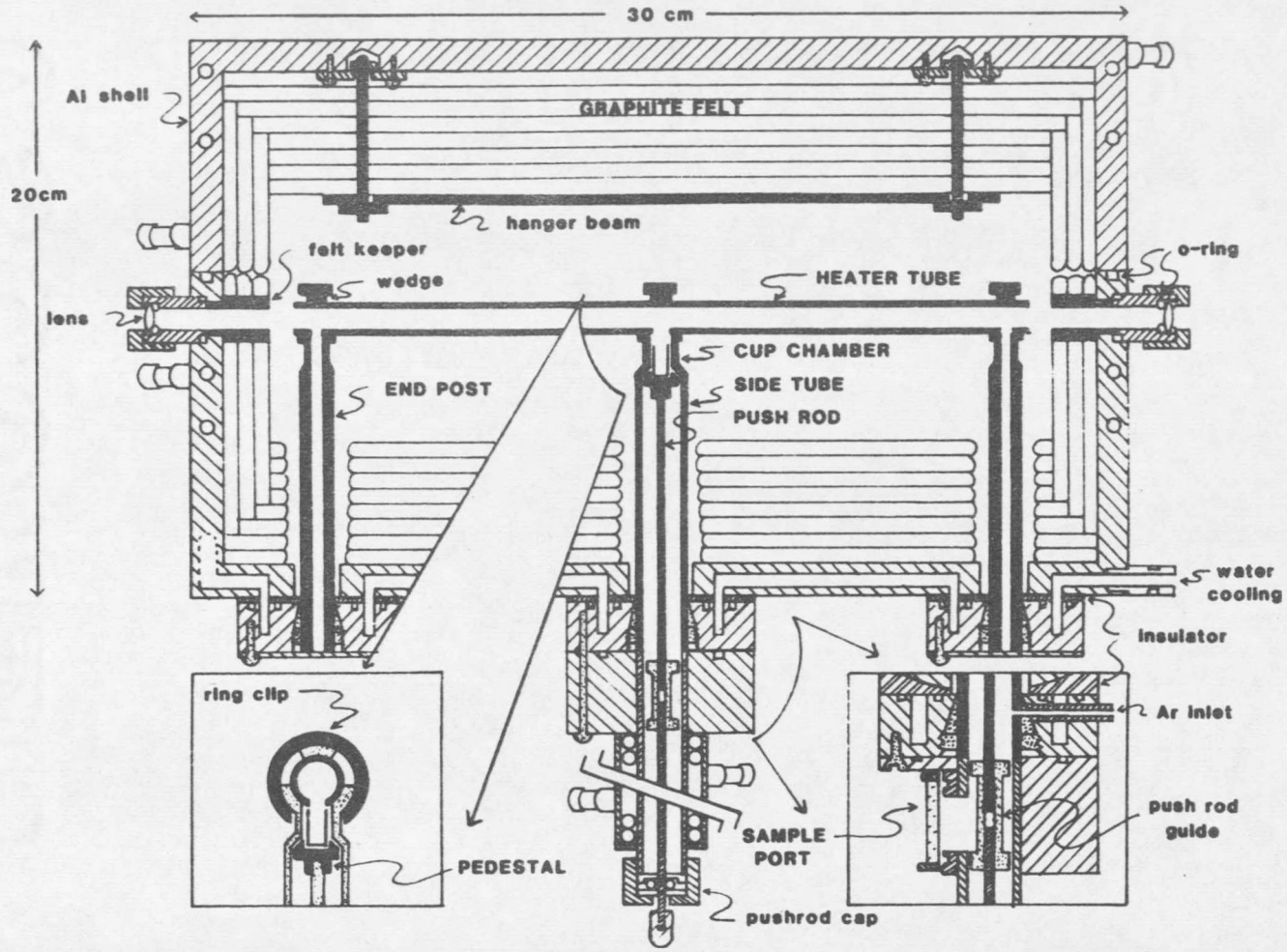


Figure 7. Cross-sectional view of a modern 3 phase constant temperature furnace.

tube being held rigidly against the pressure of the pedestal while samples are inserted. The housing surrounding the furnace was changed from a double-walled stainless steel construction to a 13 mm thick aluminum shell. This aluminum shell is drilled in such a way as to allow water to circulate throughout its interior (50). The superior conductivity of aluminum helps keep this shell cool to the touch even at internal temperatures exceeding 2500°C. The shell is cut horizontally, producing a suitcase type opening furnace for easy access to the interior parts. Previous models had end plates which had to be removed, disturbing the optical alignment, for access to the interior (46).

Three phase powering introduced new problems. At temperatures exceeding 2100°C, vertical expansion of the graphite posts becomes significant. This necessitates the alignment of the cold furnace in such a way as to compensate for thermal expansion. O-rings used to seal lenses in the furnace burned away due to the increased radiation caused by increasing the temperature on heater tube ends of post held furnaces. This problem is generally compensated for by a combination of shielding and water cooling the lens caps. Three phase powering requires addition of the side tube which re-establishes the problem of side tube contamination. However, recent studies indicate that if the side tube is made large enough to eliminate pedestal contact as samples

are inserted, this contamination problem does not occur. Physically connecting the heater tube to the two graphite end posts and side tube is difficult with post type furnaces. Heater tube contact with the end posts must be tight or arcing will occur. Connection to the side tube is more difficult than end posts because it must be manufactured tight enough to hold in sample vapor as it diffuses into the heater tube. Some of the connectors used for heater tube connection are shown in Figure 8. The one on the far right, the most recent, is easy to build but suffers from expansion effects. It holds the heater tube down on well fitting surfaces machined in the posts by pushing in a wedge which distorts the clip, putting pressure on the heater tube. As the heater tube is powered, expansion of all parts including this clip occurs. After 2100°C expansion of this clip tends to become permanent. After the heater tube is cooled the clip stays expanded, causing it to become loose and arcing may occur. Larger and larger wedges must be fitted each time the furnace is heated over 2100°C. The problem was partially remedied by making these clips more massive. Increasing the mass of these clips by three times results in only a 40°C decrease in temperature at those points where they are attached to the heater tube. These increases in mass allow the clips to be reused about three or four times above 2100°C before larger wedges are required. Other connectors using a screw type tightener also tend to suffer from

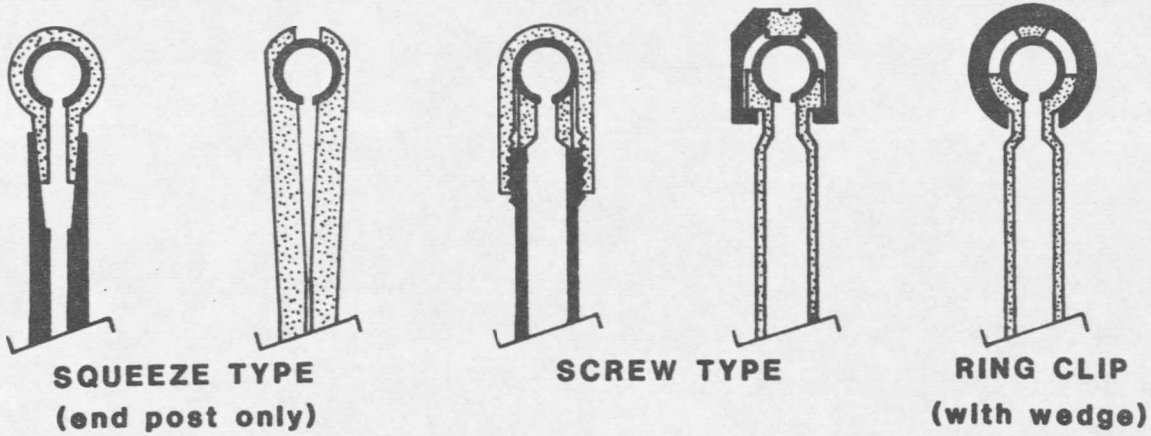


Figure 8. Cross-sectional view of graphite heater tube connectors used to hold heater tube on post type furnaces.

hysteresis. Repeated tightening of the graphite screw is a necessary operation. The end post connector shown on the far left does not suffer from expansion problems. Design of heater tube attachment is continuing.

2.2.4. Sample introduction systems

Sample introduction to these constant temperature furnaces is difficult. For a three phase powered system, the sample introduction system must: be electrically insulated from the shell, make a tight rigid contact with the side tube, keep oxygen out, stay cool to the touch, keep sample contamination at a minimum, and be easy to manipulate. The sample introduction system shown with the three phase furnace in Figure 7 is the most advanced at the time of this writing. The largest problem is cooling. When a sample is atomized, the pedestal and crucible are at furnace temperature. Lowering the hot pedestal for sample removal transfers heat to the sample port. This heat must be removed to keep the sample port from becoming too hot to handle. The pedestal must be lowered slowly to prevent the sample port window from shattering. Higher atomizer temperatures require slower sample removal rates. This limits sample cup removal time from the atomizer to about 30 sec at 2400°C. Argon is introduced into the furnace slightly above the sample port. As in earlier furnace models, argon flows out the sample window, washing oxygen off the sample

crucible when the sample is inserted. The pedestal is kept from touching the inside of the side tube, thus eliminating contamination problems as previously discussed by restricting the horizontal movement of the pushrod with a pushrod guide as shown on Figure 7.

A completely new type of sample introduction system is presently being constructed using a circular insertion motion (Figure 9). Such a system easily lends itself to automation which would be difficult with previous sample introduction systems. Work is continuing.

2.3 Operating parameters

2.3.1. Atomizer temperature

Stone (18) reported that there was a minimum furnace temperature above which a maximum absorption was observed. Above that temperature the absorption remained relatively constant. Ramelow (30) reported that above the maximum temperature the absorbance gradually decreases. Neither of these reports appears entirely correct. Studies shown in Chapter 4 indicate a more complicated picture. From this data, peak height absorbances for the 283.3 nm Pb line do appear to approach a constant absorbance at increasing temperatures, but above the value reported by Stone. A detailed account of the effect of temperature on absorbance in given in Chapter 4.

Emission from the furnace can be large at higher atomizing temperatures (particularly at longer wavelengths). The resulting

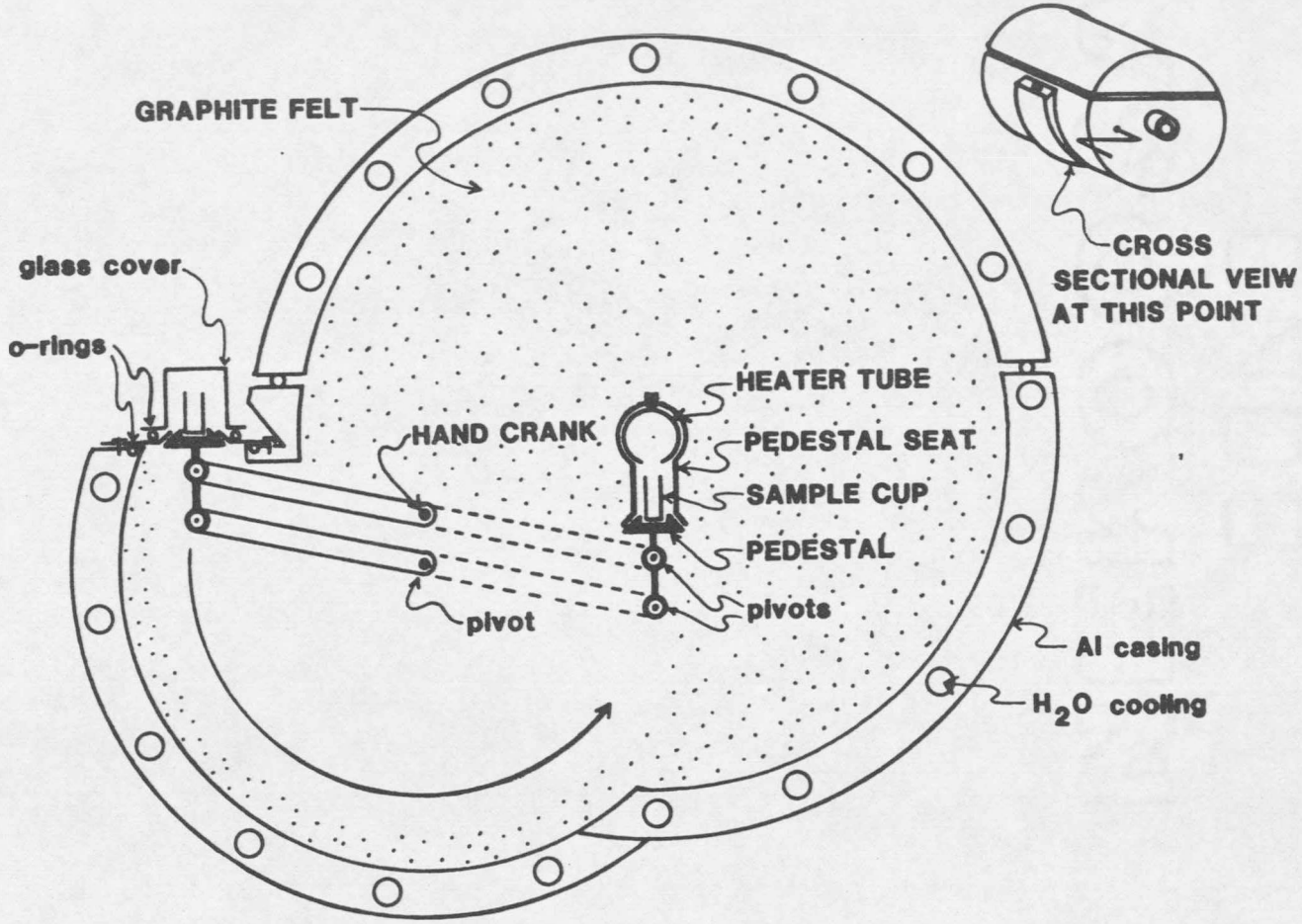


Figure 9. Cross-section view of a newly proposed furnace using a circular motion sample introduction system.

signal generated at the photomultiplier tube may create problems in absorbance computations (54,55). This furnace emission is reduced by shielding the monochromator slit with a cover plate containing a small hole. Moving the slit away from the furnace slightly greater than the focal length of the furnace lens, combined with the use of the cover plate, can bring furnace emission signals down to a manageable level (see Figure 10). The remainder of the furnace emission signal can be corrected for electronically (54,56).

2.3.2 Argon flow

The furnace is flushed with approximately three times its internal volume to assure oxygen concentrations low enough to minimize graphite part deterioration.

Early studies using peak height (18) showed that argon flow rates through the furnace had little effect on absorption signals. However, recent work using both peak height and peak area measurements show that argon flow rates do effect absorption signals. These effects are discussed in Chapter 4.

2.3.3. Sample preparation

Due to the lack of major matrix interferences in constant temperature furnaces, little sample preparation is necessary. Problems are encountered when the sample produces more background absorption than is correctable by typical background correction methods. When

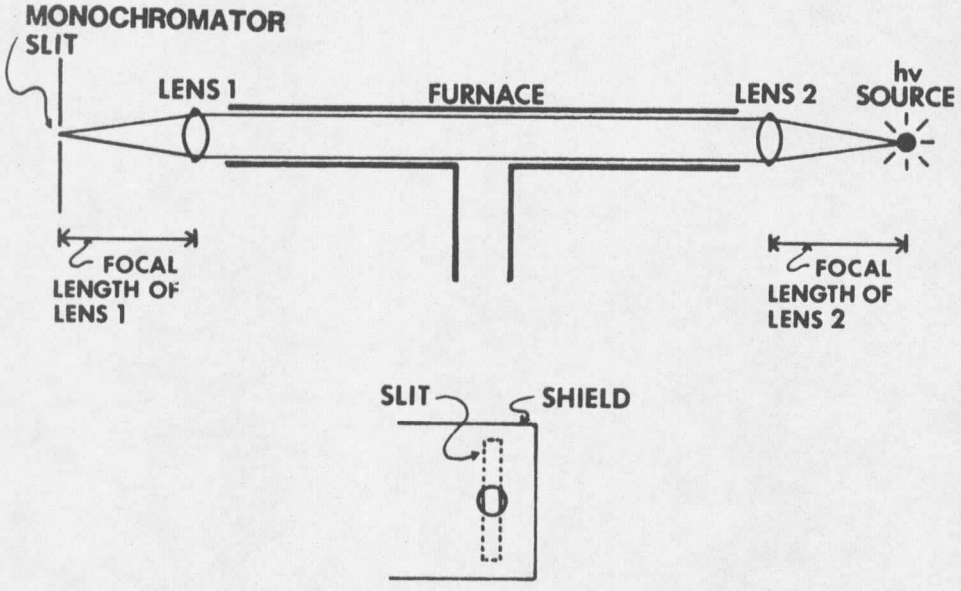


Figure 10. Diagram of the focusing system used on constant temperature furnaces. To minimize furnace emission entering the monochromator slit, the slit should be shielded as shown and the distance between lens 1 and the slit should be slightly larger than the focal length of lens 1 (too large a distance will result in decreased hv from the light source).

this happens, acid digestion or ashing is useful. Many times this is done in the graphite crucibles themselves although it greatly reduces their useable life. Another method of background reduction is to place the sample in a closed cup (52).

The three types of crucibles used in these furnaces are shown in Figure 11. The open cup crucible is generally made from hard graphite. Some open cups made from soft porous graphite are used as filters for air particulates (38), liquids (53,57), as well as gold plated for use as filters for mercury analysis (39). The closed cup used for background reduction has a porous graphite cap. Closed cups with porous bottoms have been used unsuccessfully with liquid samples. Memory effects were found on clean cups placed in racks previously occupied by cups with porous graphite bottoms. This was caused by leakage through the cup's bottoms. Another closed cup made of molybdenum or platinum was used for high temperature vapor pressure studies (51). The tapered top on this vapor pressure cell makes the seal with the seat rather than the pedestal. This assures that only atoms escaping from the orifice in the top and not through the threads will enter the atomizer tube for correct vapor pressure determinations.

Solid samples are weighed into cups prior to insertion into the furnace. Liquid samples are pipetted into cups and dried under an infrared lamp before atomization. Many samples can be dried or ashed

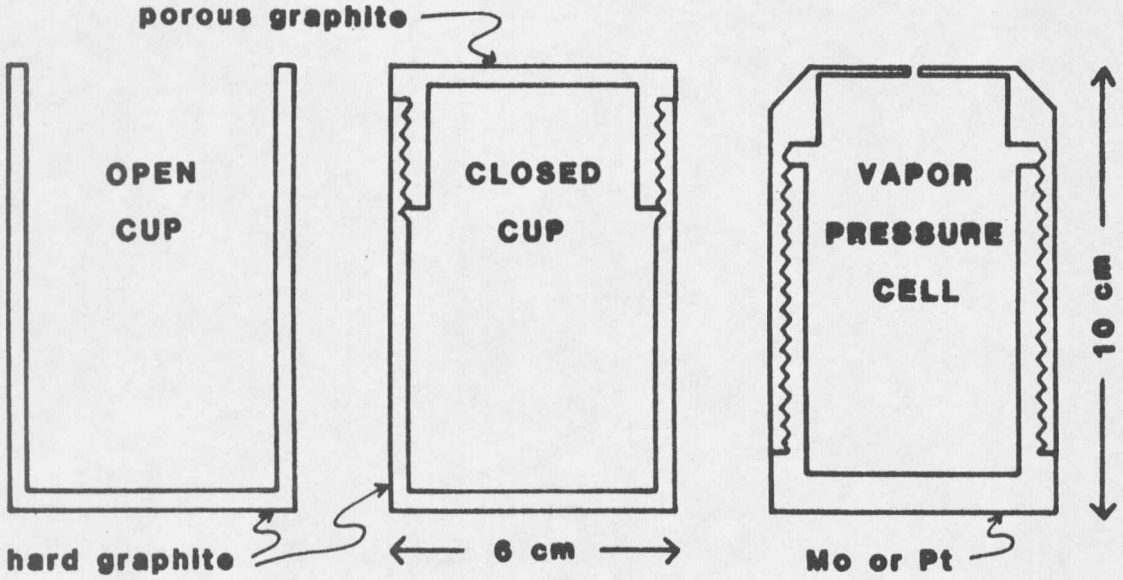


Figure 11. Types of sample crucibles used in constant temperature furnaces.

simultaneously without tying up the furnace for these routine operations.

Work described in Chapter 4 shows that differences in signals are obtained when samples are inserted into the furnace at different rates. If samples are inserted into the furnace too slowly, some atomization occurs before the pedestal mates with the seat. Samples should be inserted at a fast and steady rate to obtain the best results.

2.3.4. Sensitivity

Woodriff previously discussed absolute and relative sensitivity as it applies to tube-type atomizers (42). Absolute sensitivity, which varies inversely with the cross-sectional area of the atomizer tube, tells nothing about the sample capacity of the atomizer as a means of obtaining greater accuracy.

Chemists are often more interested in relative sensitivity: the grams of substance detectable per gram of sample. The applicability of relative sensitivity is limited because it depends on the nature of the matrix. However, it better expresses the usefulness of the device for real samples. The relative sensitivity of an atomizer, which is independent of the cross-sectional area of the tube, is directly proportional to the length of the tube. When using peak area instead of peak height (which can reduce some errors caused by matrix

materials), the relative sensitivity increases with the cube of the path length of the atomizer.

These constant temperature furnaces sometimes have greater and sometimes less absolute sensitivity than commercial pulsed atomizers depending on the element analyzed. However, their relative sensitivity is much greater due to the combination of increased path length and the ability to handle larger sample sizes. A typical graphite crucible can easily accommodate up to 200 µl of liquid or 200 mg of solid sample. Larger crucibles capable of larger sample sizes are also applicable.

Absolute sensitivity data for some elements introduced as solid samples into these furnaces are shown in Table 1. Most of this data was taken on a single phase furnace by Stone (18). Although better temperature control and better atomizer design using three phase furnaces may slightly improve these reported values, in most cases these numbers have been found to be equally applicable to the newer three phase furnaces.

Table 1. Absolute Sensitivity Data for the Woodriff Furnace.

Element	Furnace Temp (C)	Wavelength (nm)	Sensitivity (1% Absorption) (gm)
Al	2200	309.2	5×10^{-11}
Ag	1750	328.1	1×10^{-12}
		338.3	1.5×10^{-12}
Au	2200	242.8	5.1×10^{-12}
As	2200	193.7	2.5×10^{-11}
B	2300	249.8	8×10^{-7}
Be	2350	234.9	1×10^{-12}
Ca	2300	422.7	1×10^{-12}
Cd	1500	228.8	9×10^{-15}
		326.1	1×10^{-10}
Co	2400	240.7	2×10^{-11}
Cr	2300	359.4	1.5×10^{-10}
Cu	2200	324.8	2.5×10^{-11}
		327.4	5.2×10^{-11}
Dy	2200	421.2	8×10^{-11}
Er	2200	400.8	7×10^{-11}
Fe	2400	248.4	5×10^{-11}
Hg	900	253.7	3.6×10^{-11}
Ho	2200	410.4	7×10^{-11}
Mg	2300	285.2	1×10^{-12}
Mn	2200	279.4	6×10^{-13}
		280.1	2×10^{-12}
		403.1	3×10^{-11}
Ni	2350	232.0	5×10^{-10}
Pb	1750	217.0	2×10^{-12}
		283.3	1×10^{-11}
Sb	2100	217.6	1×10^{-11}
Se	2100	196.0	6×10^{-11}
Zn	1500	213.9	8×10^{-14}
		307.6	1×10^{-9}

CHAPTER 3

Supporting Electronics for the Constant Temperature Furnace

3.1 Introduction

Earlier detailed studies of the constant temperature furnace was stifled by poor supporting electronics and electronic data handling. These earlier constant temperature furnace systems were often put together with mismatched and poorly maintained electronic equipment which added to atomic absorption measurement inaccuracies. Background correction was either non-existent or had to be hand calculated from simultaneous reference line tracings in a two channel monochromator system. A good stable electronic system was greatly needed for accurate studies using constant temperature furnaces. The following sections describe the design and operation of supporting electronics for constant temperature furnaces made from modern inexpensive integrated circuit chips.

3.2 A Stable Pulsed Hollow-Cathode Power Supply

3.2.1 Introduction

Optical choppers and rotating mirrors have traditionally been used to interrupt hollow-cathode light sources used in atomic absorption spectroscopy, and to switch between sample and reference light sources in background corrected systems. Commercial pulsed hollow-cathode

power supplies have been utilized for the same purpose. The power supply described in this section, however, is much less expensive and at least as stable as commercially available units (for example, the 0.0082% stability of this unit compares favorably with the 0.05% stability figure published for the Spectrogram corporation Model LPA-ID hollow-cathode power supply). This power supply consists of an unregulated 400 volt DC power supply and a programmable constant current regulator which drives a hollow-cathode or hydrogen lamp. The lamp is switched from a very low "idle" level to a high emission level by digital logic signals. Both "idle" and "on" levels for each channel are adjustable by front panel potentiometers. The power supply provides a high level of current regulation and emission stability ($\pm$0.0082%) with large changes ($\pm$40 volts) in lamp supply voltage. The parts cost of the system is minimal - less than $20.00 plus an unregulated 400 volt DC power supply. It may be used to replace the optical chopper or commercial pulsed hollow-cathode power supplies in conventional atomic absorption systems using lock-in amplifier data acquisition.

3.2.2 Circuit Description

The basic regulator circuit, sketched in Figure 12, may be understood by following its operation from the time the hollow-cathode lamp high voltage supply is turned on until the lamp current is

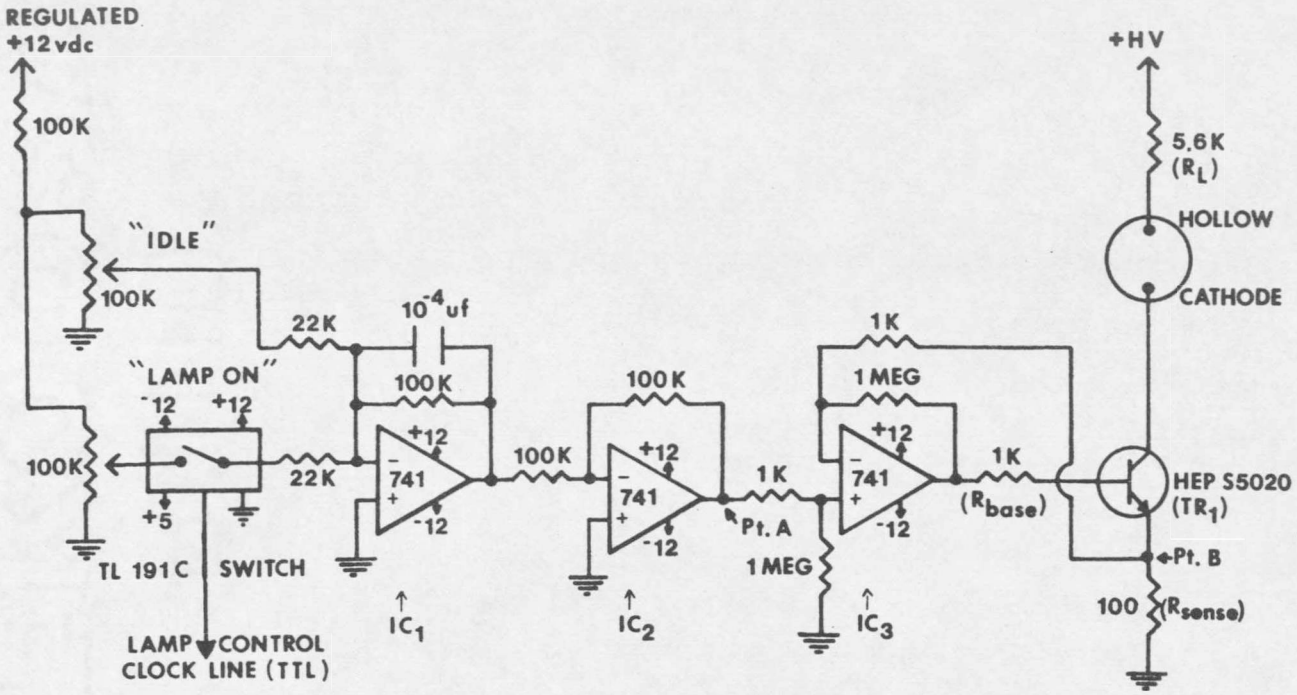


Figure 12. The circuit diagram for the pulsed hollow-cathode power supply. The regulated 12 volt reference supply provides a stable reference voltage for the "idle" and "lamp on" controls. These voltages are summed by IC_1 when the "lamp on" switch is closed. The output of IC_1 is returned to positive polarity by inverting amplifier IC_2, and presented as a reference signal to the non-inverting input of control amplifier IC_3. Lamp current is sensed by observing the voltage drop across R_{sense}; this voltage is compared to the programmable reference voltage by control amplifier IC_3. The output of this amplifier controls the electron flow through regulator transistor TR_1. Lamp current will rise until the IR drop across R_{sense} almost exactly equals the reference voltage at point A.

stabilized. Let us begin by assuming that switch S_1, the "lamp on" switch is open. The input of summing amplifier IC_1 will then be a positive voltage set by the "idle" potentiometer, producing a negative input to inverting amplifier IC_2, and a positive voltage at the non-inverting (+) input of control amplifier IC_3 (point A). At this time the lamp has not yet fired; no current is flowing through the lamp circuit, and the voltage across the current sensing resistor R_{sense} (point B) is zero. With zero input voltage into the inverting (-) input of control amplifier IC_3 and a positive voltage applied to its non-inverting (+) input, the output of IC_3 will be at its positive limit, about +12 volts. Transistor TR_1 will thus be gated full "on", and will provide very little resistance to current flow in the hollow-cathode lamp circuit.

If the high voltage supplied to the hollow-cathode lamp is sufficient to fire the lamp (around 400 volts), current will begin to flow in the R_L-TR_1-R_{sense} circuit, and a voltage drop E_{sense} equal to

$$E_{sense} = (\text{hollow-cathode current}) \quad (R_{sense})$$

will develop at point B. This positive voltage is applied to the inverting input of control amplifier IC_3, thus reducing the positive output of this operational amplifier and reducing the drive to the regulator transistor TR_1. The current through the hollow-cathode lamp will increase until the voltage developed at point B (E_{sense}) almost

exactly equals the control voltage (E_{Ref}) at point A. As the voltage developed at point B approaches the reference voltage presented at point A, the output of control amplifier IC_3 falls, thus limiting the current through the hollow-cathode lamp circuit. If for any reason the current in the lamp circuit should decrease (a decrease in the DC high voltage supply, for example), the difference between E_{Ref} and E_{sense} will increase, the output of IC_3 will become more positive, and the effective resistance of the regulator transistor TR_1 will decrease causing it to pass more current.

A mathematical description of this circuit is relatively straightforward:

a) The voltage at point B is given by the equation

$$E_{sense} = (I_{lamp})(R_{sense})$$

b) The control amplifier output (IC_3) is given by the equation

$$E_{control} = (E_{Ref} - E_{sense})(\text{Control amplified gain})$$

Control amplifier IC_3 is a differential operational amplifier operated with a gain on the order of 10^3 at low frequencies.

c) The lamp current through the transistor regulator is given by the equation

$$I_{lamp} = (\text{Transistor base current})(\text{Transistor current gain})$$

where

$$\text{Transistor base current} = \frac{E_{control}}{\text{Transistor base resistor } R_{base}}$$

Combining these equations, we find that

$$I_{lamp} = \frac{(E_{control})}{R_{base}} \text{ (Transistor current gain); or}$$

$$I_{lamp} = \frac{(E_{Ref}-E_{sense})\ \text{(amplifier gain)}}{R_{base}} \text{ (Transistor current gain);}$$

or

$$I_{lamp} = \frac{(E_{Ref}-[(I_{lamp})(R_{sense})]\,\text{(Amplifier gain)}}{R_{base}} \text{ (Transistor current gain).}$$

Rearranging this equation, we find that

$$[E_{Ref}-(I_{lamp})(R_{sense})] = \frac{(I_{lamp})(R_{base})}{\text{(Amplifier gain)(Transistor current gain)}}$$

Substituting values for a lamp current of 10 milliampers, a sensing resistor of 100 ohms, a transistor base resistor of 1 K ohms (R_{base}), an amplifier gain of 10^3, and a typical transistor current gain of 40, we find that

$$[E_{Ref} - (10^{-2}\ \text{amp})(10^2\ \text{ohm})] = \frac{(10^{-2}\ \text{amp})(10^3\text{ohm})}{(10^3)(40)}$$

$$E_{Ref} - 1.000 \text{ volt} = 2.5 \times 10^{-4} \text{ volts}$$

$$E_{Ref} = 1.00025 \text{ volts}$$

Assuming the typical gain figures presented above, the reference voltage must exceed the voltage developed across the current sensing resistor by about 250 microvolts to maintain a 10 milliampere current though the hollow-cathode lamp. A change in lamp current of 1 microampere (1 part in 10,000 or 0.01% for a 10 ma lamp current) will

produce a change in control amplifier input of (10^{-6} amp)(10^{2} ohms) = 10^{-4} volts, resulting in a change in control amplifier output of (10^{-4} volts)(10^{3} gain) = 0.1 volt. This ability to make large corrections in the transistor control voltage with minute changes in lamp current causes the circuit to maintain the hollow-cathode lamp current at an extremely stable value. Other factors, principally the regulation of the control voltage to the non-inverting input of IC_3 and the stability of the current sensing resistor R_{sense} have limited the measured long term stability of this circuit to a relative standard deviation of about ±0.0082%.

Current regulation was measured using the circuit illustrated in Figure 13. The voltage drop across the sensing resistor R_{sense} was monitored by a voltage to frequency converter (Analog Devices AD 452J 100 Khz unit, stability equal to a relative standard deviation of about ±0.0042%) and the digital output from this unit accumulated in a scaler. The lamp was pulsed by a 100 hz TTL signal derived from a 5 Mhz crystal oscillator and divider string (Figure 14), and a preset counter gated the scaler "on" for 200 lamp pulses. Results of this experiment are presented in Table 2.

3.2.3 Applications

This system has been applied to drive a single hollow-cathode lamp in a flameless atomic absorption system using a DC powered hollow-

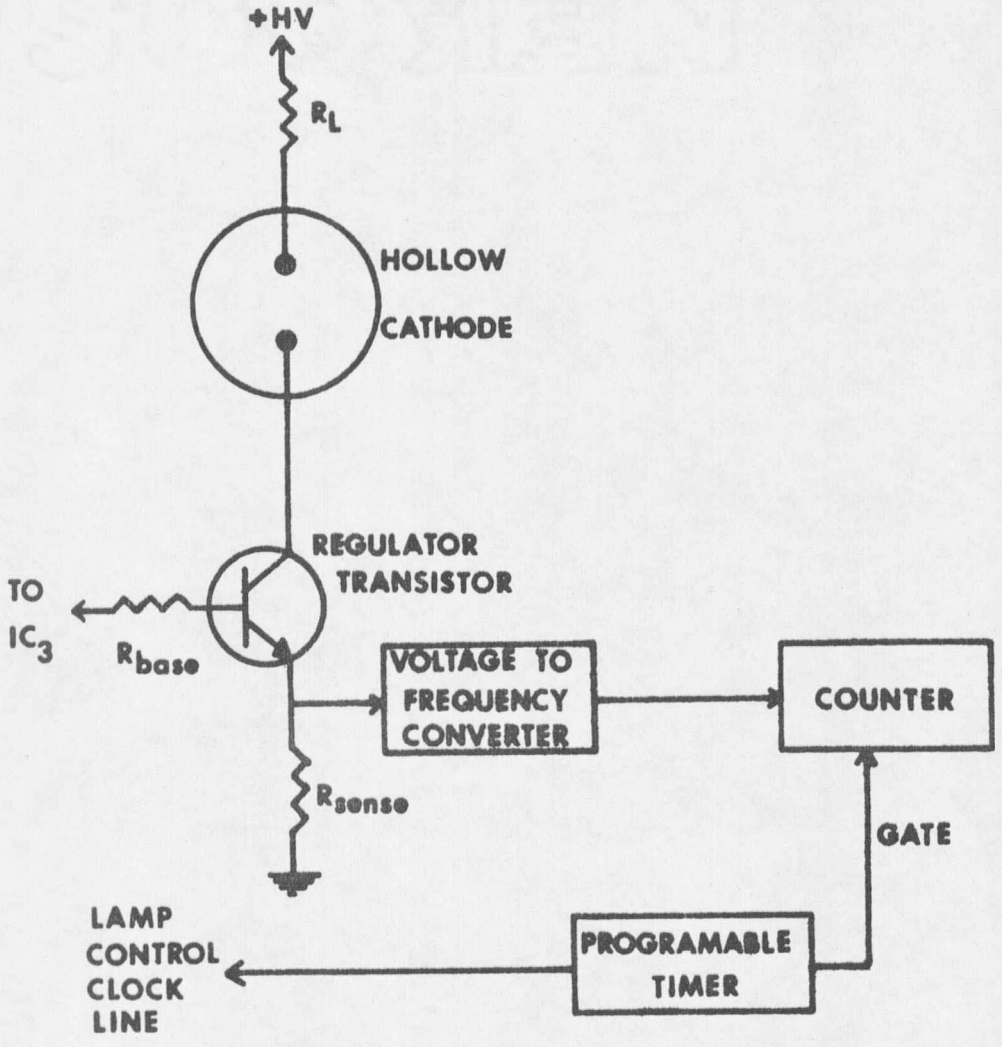


Figure 13. Current stability was monitored by this circuit. A voltage-to-frequency converter digitized the voltage drop across the sensing resistor; this digitized signal was accumulated in a scaler. The lamp was pulsed by a 100 hz crystal-controlled clock; data was collected for 200 lamp cycles.

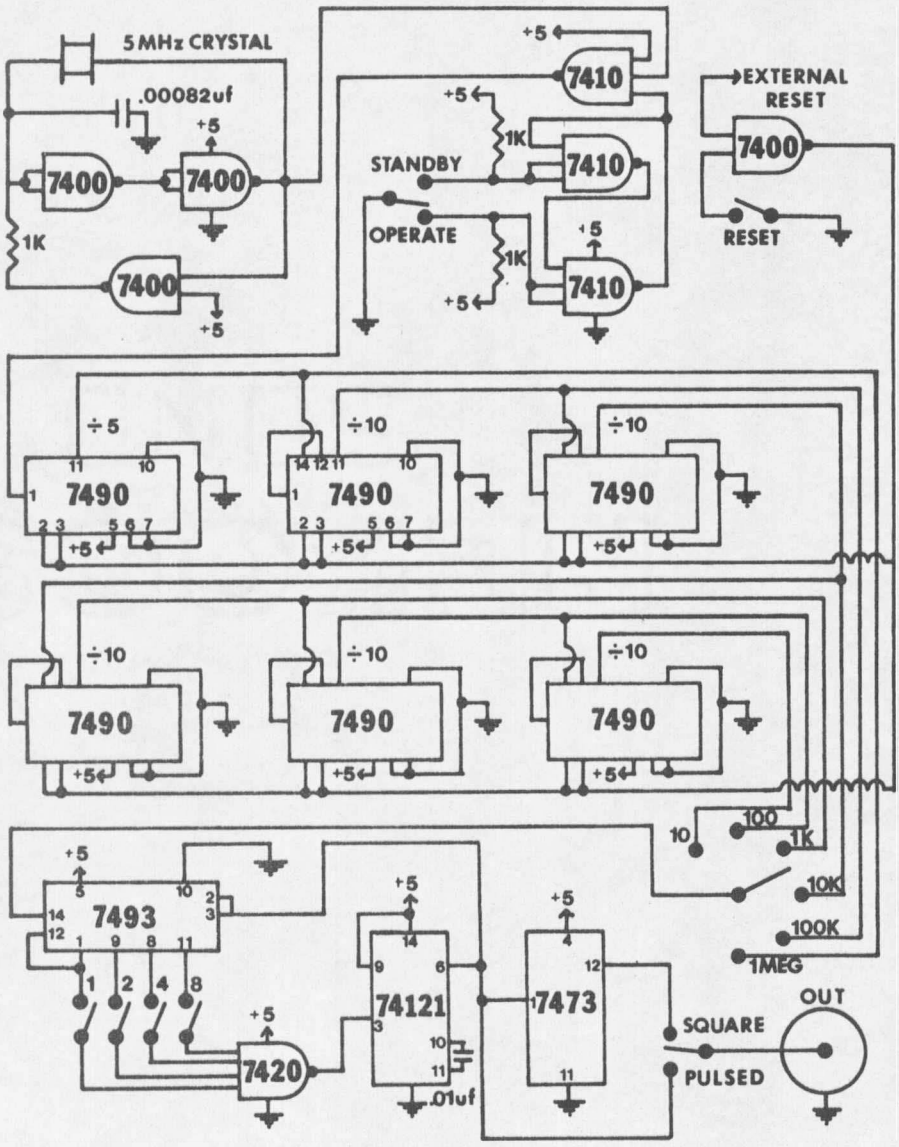


Figure 14. Crystal clock (1 Mhz to 1 hz output capability)

Table 2. Performance of the Pulsed Hollow-Cathode Light Source.

Experimental Conditions:

Hollow-cathode lamp: Cu

Operating current: 10 ma

Operating frequency: 100 hz

Sample size: 200 pulses

DC Power Supply Voltage	320	340	360	380	400
Number of Measurements	15	15	15	15	15
Signal (Average Counts)	46835.7	46838.8	46841.0	46843.9	46846.1
Standard Deviation	2.0702	0.0000	1.1952	1.8898	2.0702
% Standard Deviation	0.0044	0.0000	0.0026	0.0040	0.0044

Total count variation with 320-400 volt power variation:

n = 75

Av = 46841.1

Standard Deviation = 3.8555

% S. D. = 0.0082% variation

cathode lamp, an optical chopper, and a lock-in amplifier. Some trouble had been encountered with this system (Figure 15), since light from the hot sample atomizer was passing through the chopper blades, reflection from the window of the hollow-cathode lamp, and returning as chopped broad-band light to the spectrometer and data acquisition system. The optical chopper was removed from the system and the regulated DC hollow-cathode power supply replaced by the current regulated pulsed hollow-cathode power supply. Although light from the atomizer still struck the lamp window and returned to the spectrometer slit, it was not chopped and the lock-in amplifier did not respond to it. This improvement was made more attractive by the fact that an expensive regulated hollow-cathode power supply was replaced by an inexpensive unregulated DC supply, and the $600 optical chopper was replaced by an inexpensive pulsed current regulator.

3.3 A Background Emission Correction System for Atomic Absorption Spectroscopy

3.3.1 Introduction

Two major problems are encountered during the measurement of a sample's absorbance in an atomic absorption spectrophotometer. One is the problem of broad band absorption by gaseous molecular species in the optical path. The other is broad band emission by the sample atomization chamber when operated at high temperatures. The problem of

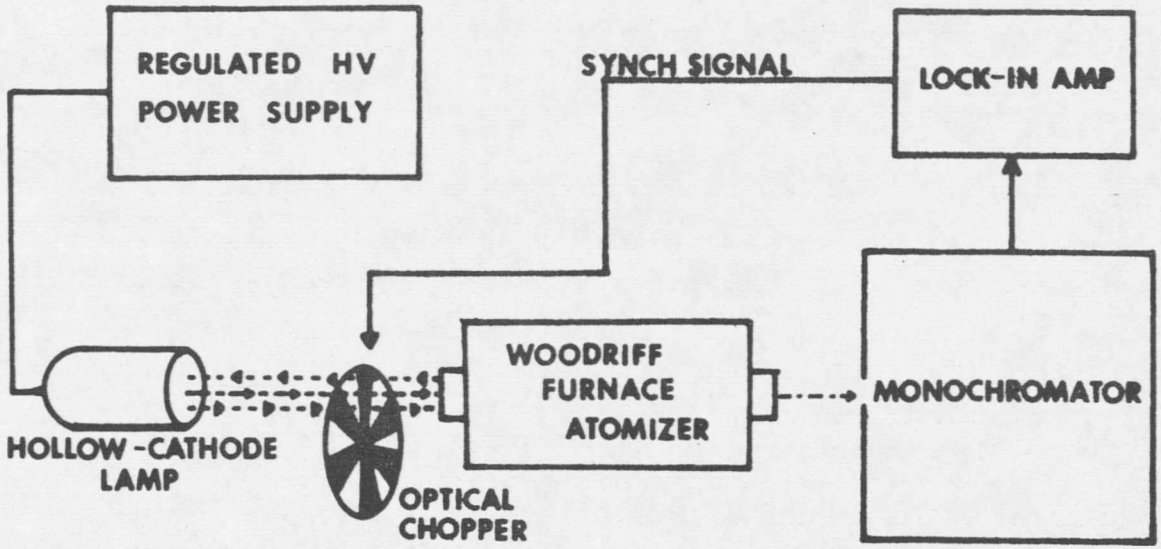


Figure 15. Elimination of interference from furnace background light. The conventional system had been bothered by light from the furnace passing through the chopper blades, reflecting from the lamp window, and returning to the spectrometer as chopped broad-band light. The pulsed hollow-cathode system eliminated this problem and resulted in increased stability and more than an order of magnitude reduction in the cost of the light source (power supply, hollow-cathode lamp, and optical chopper system).

broad band absorption by gaseous molecular species has been handled in a variety of ways, including the Hitachi Zeeman effect (58-62), various wavelength modulation techniques (63-68) and dual channel techniques (69-71). The technique most commonly used and which has been subsequently adopted by most all manufacturers of atomic absorption instruments for the correction of broad band absorption was first described by Koirtyahann and Pickett (72,73). In this technique the problem of broad band absorption is handled by directing a broad band reference signal (H_2 light) through the sample. If the spectral bandpass of the monochromator is large with respect to the band width of the atomic absorption line, absorption will be principally broad band. Absorption of the atomic species plus the gaseous molecular species is determined by passing atomic light from an appropriate hollow-cathode lamp through the sample. The background corrected absorbance is calculated by substracting the logarithm of the hollow-cathode lamp signal from the logarithm of the broad band reference lamp signal. It should be pointed out, however, that as the spectral bandpass of the monochromator approaches the band width of the atomic line the fraction of reference light on that atomic line becomes increasingly larger. Under these conditions inaccurate background correction results. A possible solution to this overlap problem is to use sequential hollow-cathodes (44). In this system the reference

light passes through the elemental hollow-cathode where the atomic line portion of the reference signal is removed by sputtered atoms present inside the elemental lamp. This type of system could be very useful for situations where very narrow spectral bandpasses are required.

Siemer (55) has pointed out that errors can arise if the unmodulated atomic, black-body and molecular emission signals are not corrected for prior to logarithmic conversion. In electrothermal atomizers this background emission signal can be very large at higher atomizing temperatures (particularly at longer wavelengths) and must be eliminated before the absorbance computation.

An integrating background correction system was described by Donnelly et al. (56). This system was based on a four phase operational cycle with data acquisition occurring during two of the four phases and analog computation during the other two phases. Donnelly's system compensated for sample chamber emission by using AC coupling at the input to the photomultiplier preamplifier.

The background emission correction system described in this chapter is based on work earlier reported by Amend (74,75). It, as in the Donnelly system is also based on a four phase operation cycle but measures the background emission of the hot sample container in the absence of all other signals during one phase of its cycle. This signal is then subtracted from reference and atomic line signals

acquired during the two subsequent phases of the cycle, before converting these values to logarithms for the absorbance computation. Analog computation takes place while data is being acquired, thus increasing the total time available for data acquisition.

3.3.2 Circuit Description

The circuit diagram for the BECS unit is presented in Figures 16 and 17. Figure 16 comprises the timing section while Figure 17 presents the computation section of the BECS. Figure 18 illustrates the various timing outputs of the timing section which drive the electronic switches in both the lamp power supplies and the computation section of the BECS. Figure 19 illustrates the activity of the integrators in the computation section of the BECS.

Operation of the system is based on a four phase cycle derived from a TTL SN74155 decoder driven by a 7473 dual flip-flop and an external crystal clock pulse. The 74155 decoder produces four equally spaced negative logic signals. The first three are inverted to positive logic by NAND gates (TTL 7400). These three positive true signals provide the logic necessary to close the appropriate switches in both the HC and H_2 power supplies and in the computation section of the BECS. The fourth signal is used to generate short "data transfer" and "reset" pulses by triggering monostable multivibrators, A, B and C. Monostable multivibrator A generates the "data transfer" pulse.

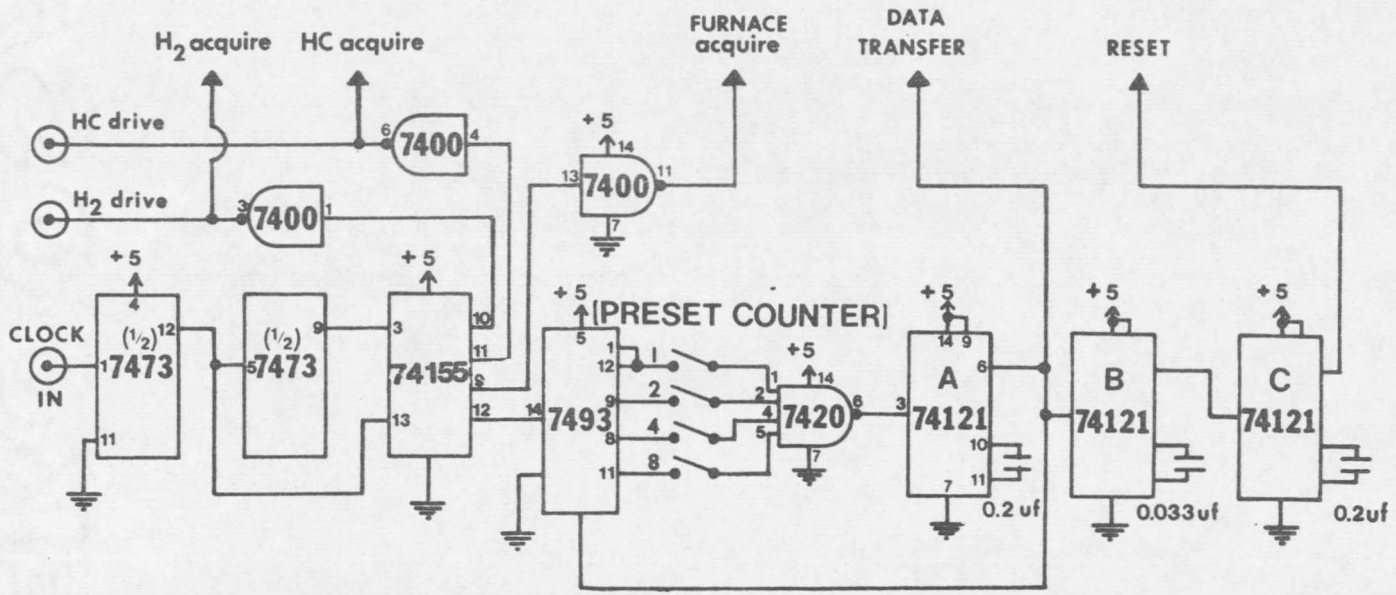


Figure 16. The circuit diagram for the timing section of the BECS. Of the four equally spaced logic signals produced from the 74155, three are used to close switches in the H_2 and HC lamp power supplies and in the computation section of the BECS. The last logic signal is used to trigger a series of monostable multivibrators which generate successive "data transfer" and "reset" pulses.

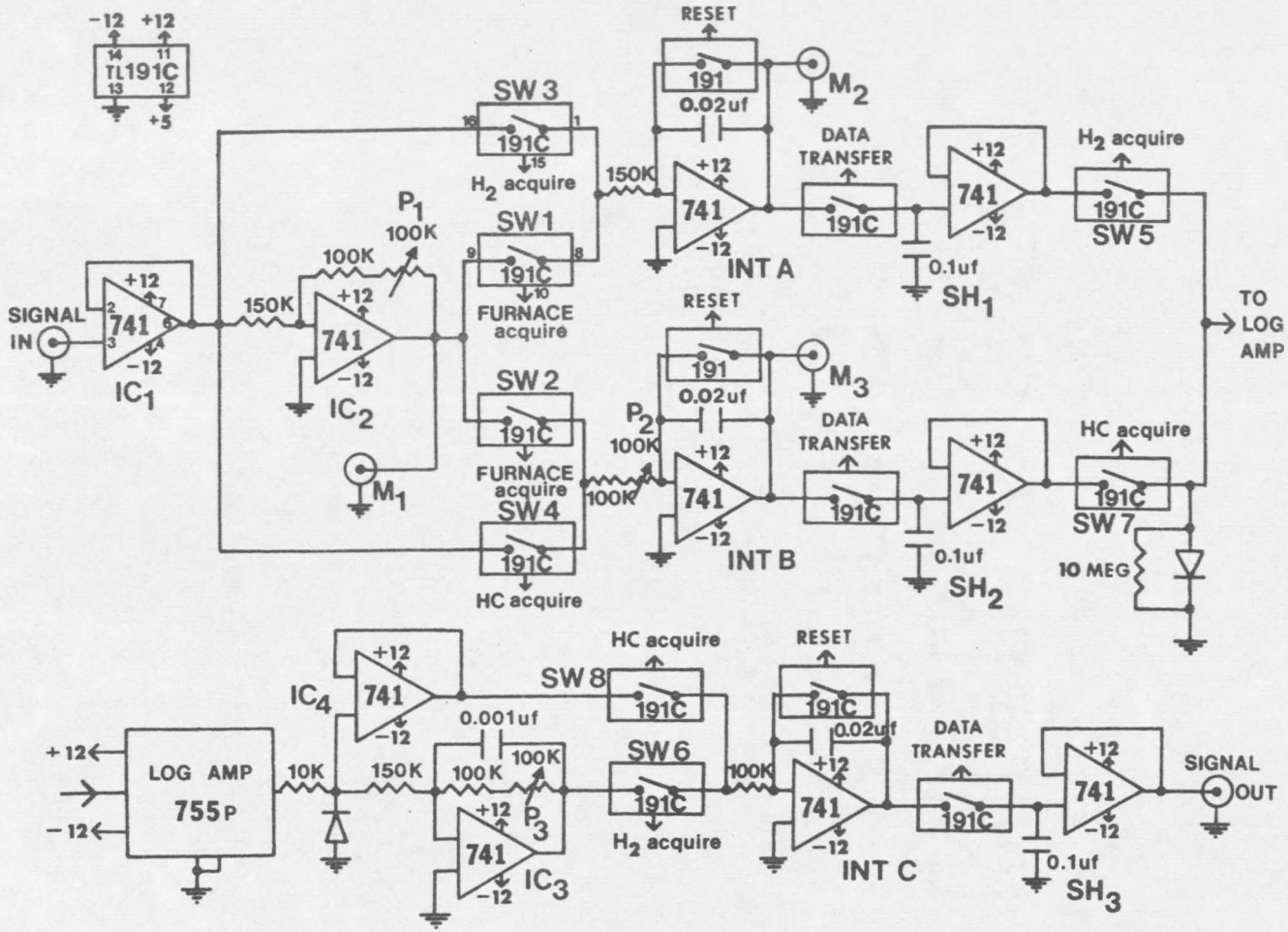


Figure 17. The circuit diagram for the computation section of the BECS. An amplified P-M tube signal is presented at the "signal in," while the absorbance signal is produced at "signal out" and may be fed to a recorder or a V-F converter and scaler for digital integration.

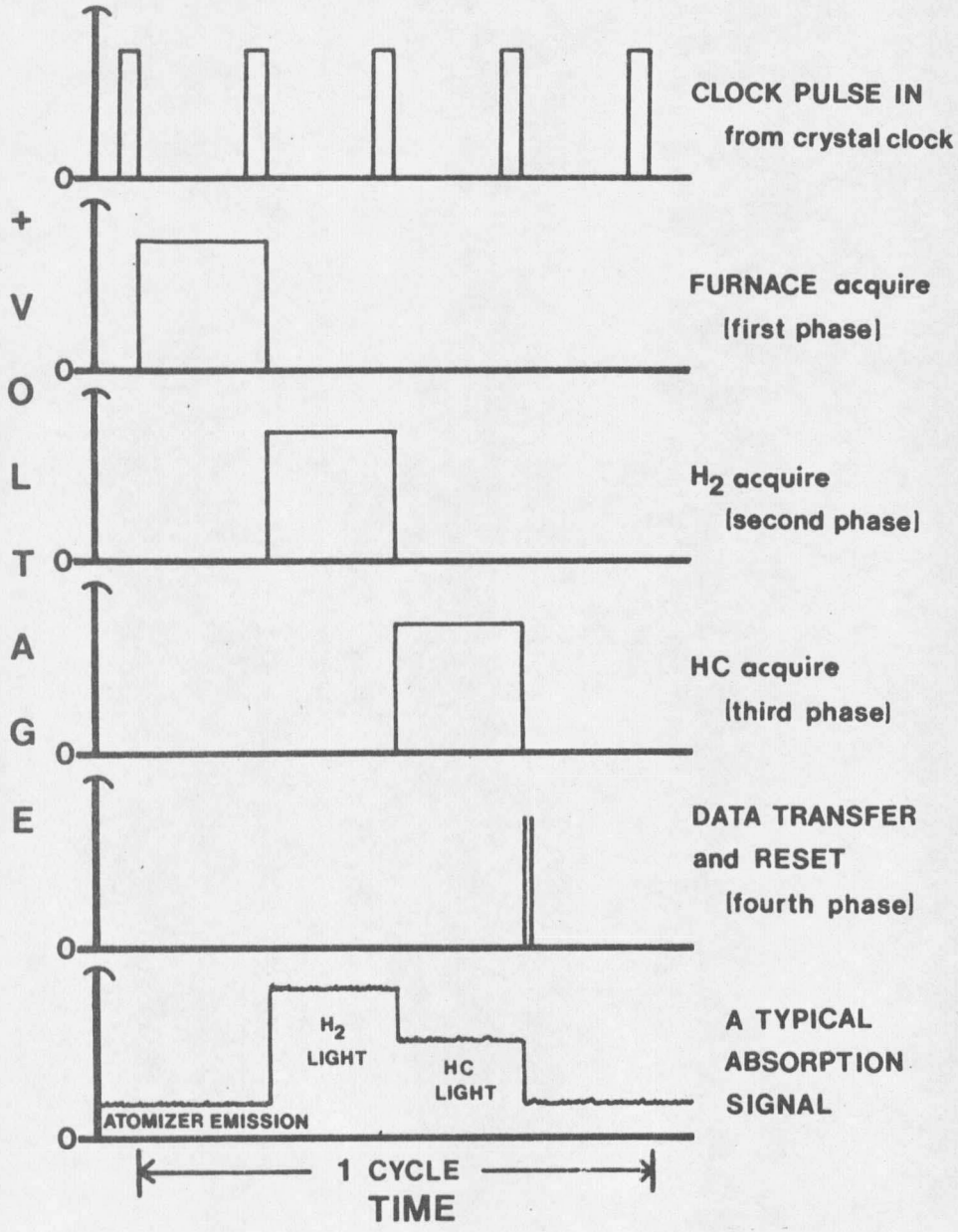


Figure 18. The various outputs of the timing section of the BECS with respect to the crystal clock time marks.

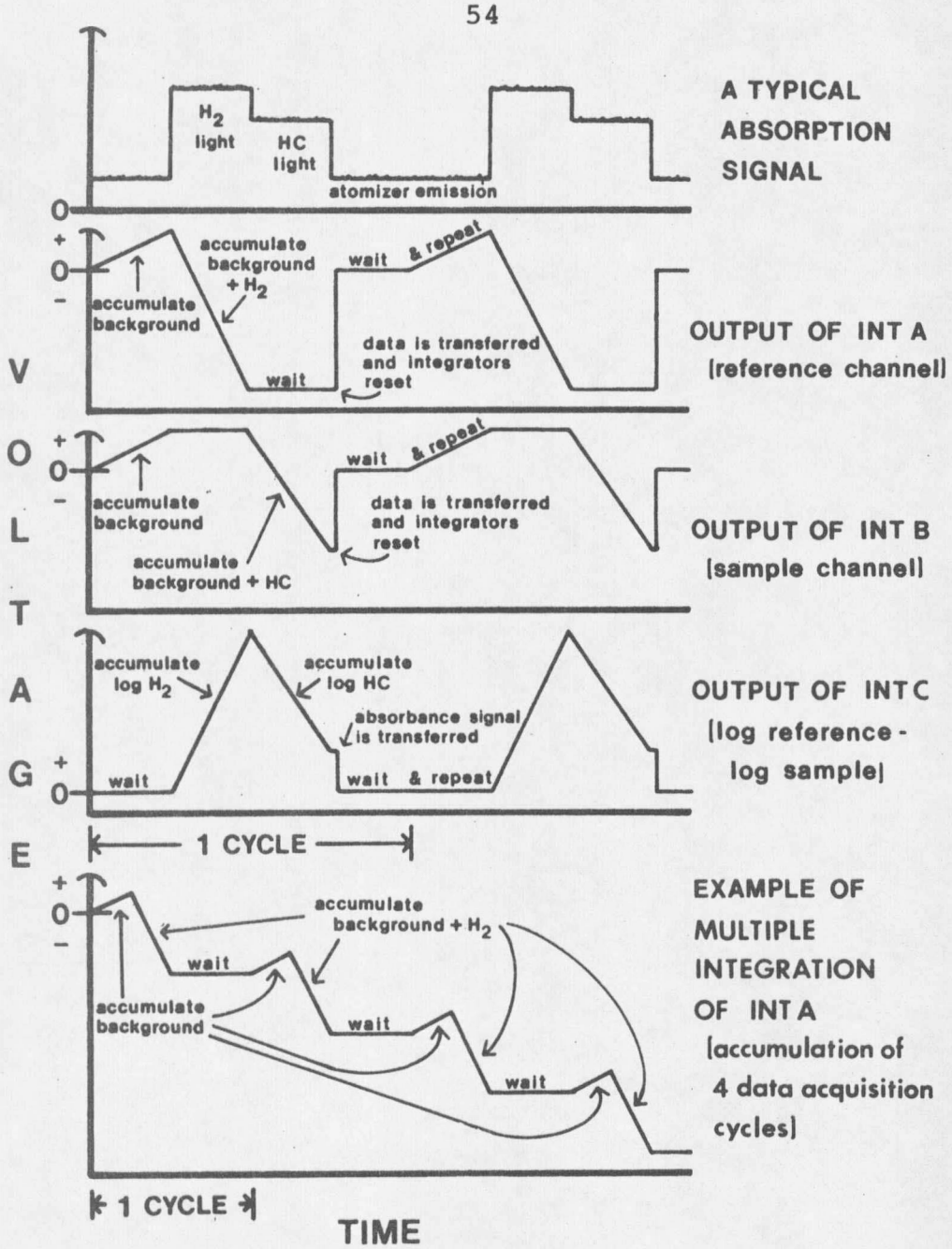


Figure 19. The outputs of the three integrators in the computation section of the BECS. A typical absorption signal (presented at the top of this figure) is integrated as shown by the three different integrators. The graph at the bottom shows the effect of setting the preset counter in the timing section of the BECS to four.

Monostable multivibrator B provides a 30 μsec delay which assures that all data is transferred before the integrators are reset by monostable C. Note that a preset counter preceeds monostables A, B and C. This feature allows 1 to 15 separate measurements to be integrated in integ rators INT A, INT B and INT C before the data is transferred through the BECS (see Figure 19).

In the first phase of the four phase cycle, both hydrogen reference lamp (H_2) and the atomic line sample lamp (HC) are allowed to "idle" at a very low light output since both H_2 and HC lamp drives are in a "0" logic state. During this first phase only the "furnace acquire" output is active causing switches SW 1 and SW 2 to be closed. An incoming furnace (or sample atomization chamber) background emission signal is routed through IC_2 and is integrated by integrators INT A and INT B. Note that this signal is inverted in sign by IC_2 before application to the integrators. During the second phase of the cycle the "H_2 acquire" goes to logic "1" which turns on the hydrogen reference lamp and closes switch SW 3. A signal equal to reference plus background emission is then accumulated by integrator INT A. Since the inverted integrated background emission signal remained in the integrator, at the end of this phase INT A content will be equal to [(reference signal + emission background) - (emission background)] = reference signal. During the third phase of the cycle the "HC acquire"

goes to logic "1" turning on the hollow-cathode sample lamp, closing switch SW 4 and a similar accumulation of the atomic line sample signal takes place. At the end of this phase INT B content will be equal to [(sample signal + emission background) - (emission background)] = sample signal. During the fourth and final phase of the cycle these signals are transferred to sample hold circuits SH_1 and SH_2, the integrators are reset and the data acquisition cycle is repeated.

During the second phase of the next acquisition cycle, switches SW 5 and SW 6 close, transferring the emission corrected reference signal through the 755P logarithmic amplifier and the inverting amplifier IC_3. This signal is integrated by integrator INT C. During the third phase of this next acquisition cycle, switches SW 7 and SW 8 close, transferring the emission corrected atomic line sample signal through the 755P logarithmic amplifier and the non-inverting follower amplifier IC_4. This signal is integrated by integrator INT C. At the end of this phase the output of INT C will be equal to [(log reference signal - log sample signal)] = log Io/I = absorbance. During the fourth phase of this next acquisition cycle this absorbance signal is transferred to sample hold SH_3 and the integrator is reset. The output of the BECS at this point is proportional to the absorbance of the sample data receive in the previous cycle. At reasonably fast clock rates this one cycle lag time in the signal received and the absorbance

signal produced by the BECS presents no problems in practical analysis.

In order to assure proper operation of the BECS several criteria must be met:

a) All input signals to the BECS must be of positive polarity.

b) Potentiometer P_1 must be adjusted so the magnitude of the input signal (at the ouput of IC_1) matches the signal at the output of IC_2 (M_1) but is opposite in polarity.

c) Potentiometer P_2 must be adjusted to assure that the RC time constant of integrator INT B matches that of INT A. This can be accomplished by monitoring both integrators at M_2 and M_3 and adjusting P_2 until equal integration is achieved when both reference and sample signals are equal.

d) Finally, potentiometer P_3 must be adjusted, to make the gain of amplifier IC_3 equal to -1.00. The output voltage of the BECS will then be zero when both reference and sample signals are equal.

e) The system may be conveniently set up using an oscilloscope to monitor the lamp and furnace emission signals at the input of the BECS.

3.3.3 Experimental Results and Discussion

A block diagram of the system is presented in Figure 20. A Woodriff furnace electrothermal atomizer was used for the sample

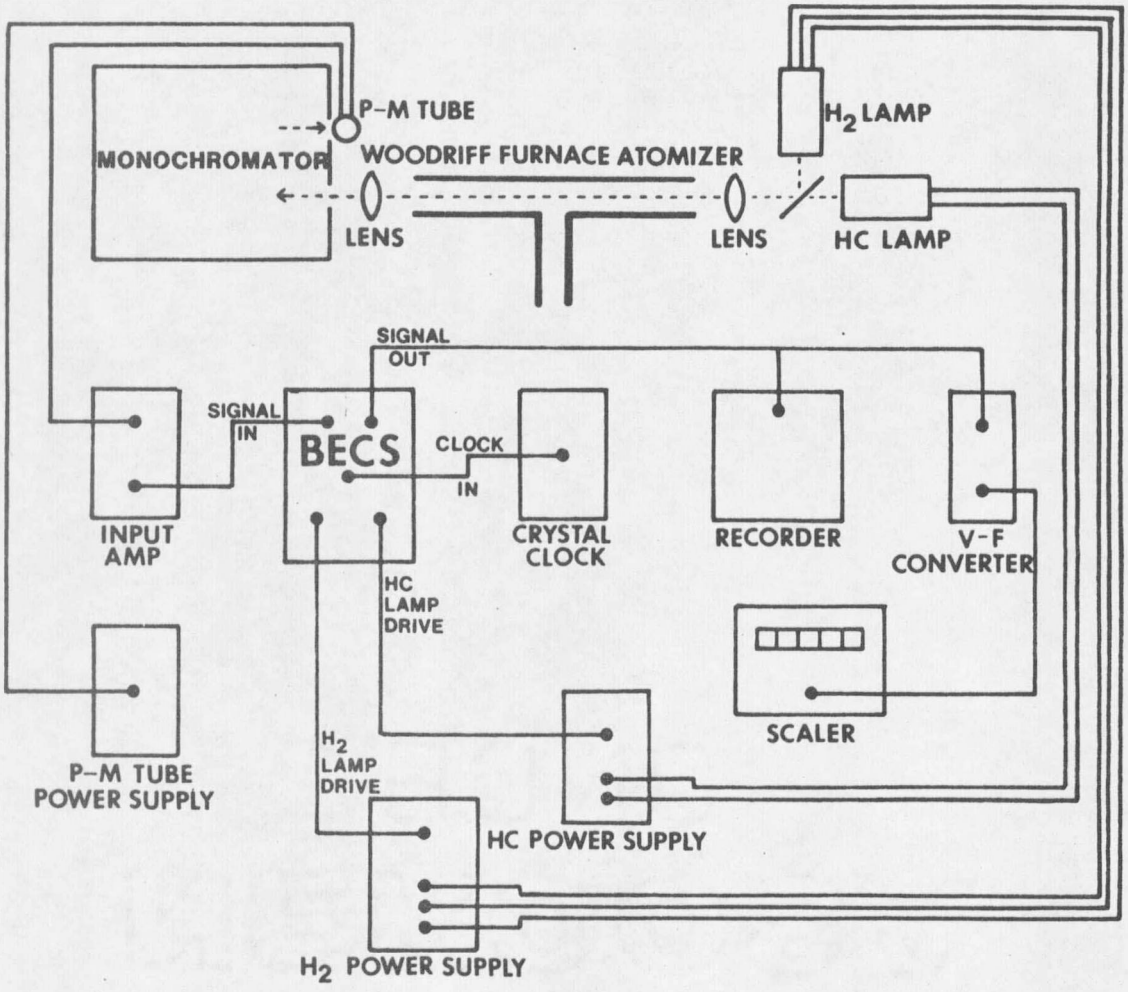
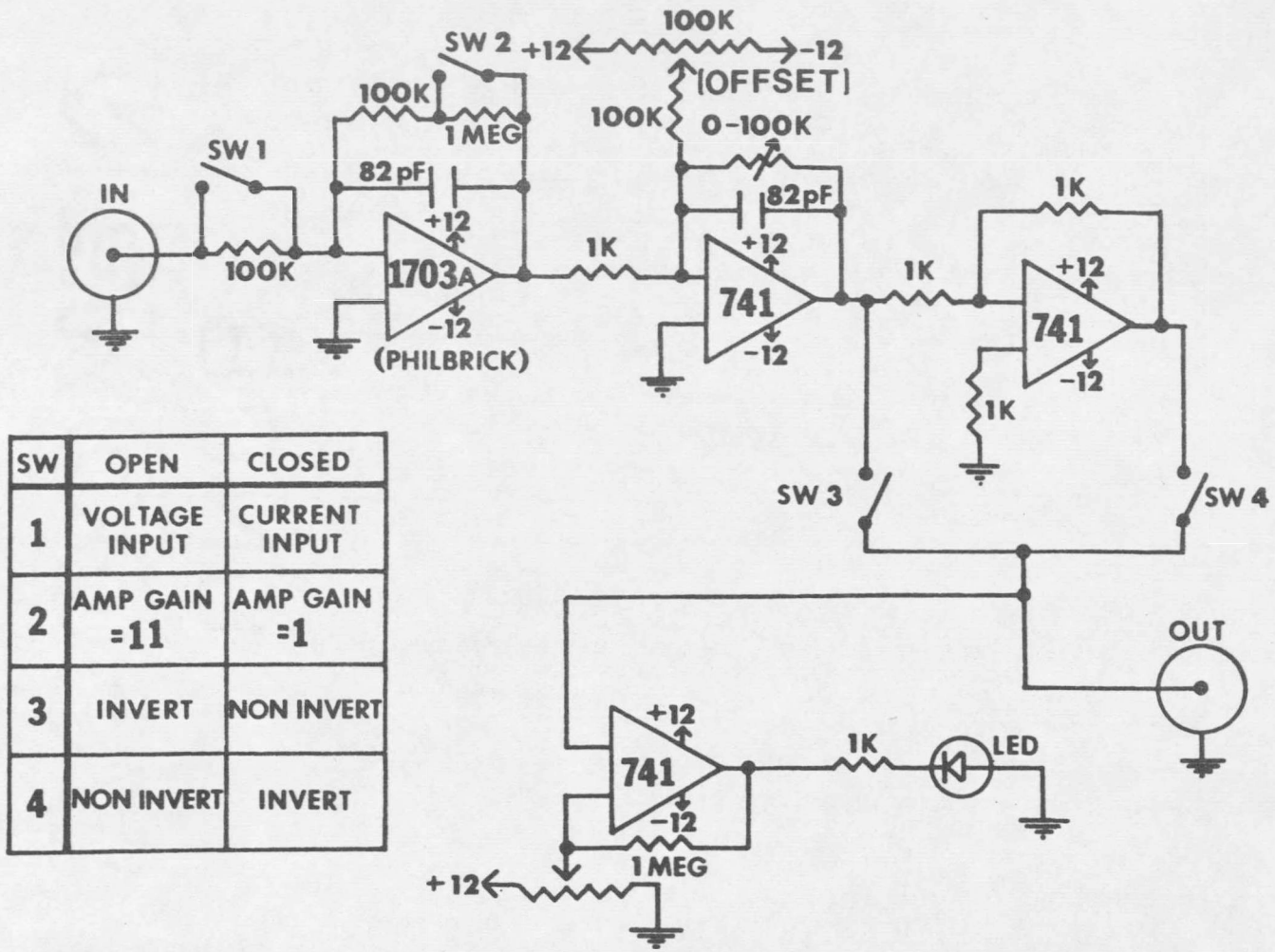


Figure 20. The overall system diagram.

atomization chamber. The P-M tube was a RCA IP106 powered by a Fluke 412 high voltage power supply. A Beckman DU type monochromator with a 0.10 mm slit was also utilized. The circuit of the input amplifier is illustrated in Figure 21 and was operated in an inverting current follower mode. The circuit of the voltage to frequency (V-F) converter is illustrated in Figure 22. The crystal clock and hollow-cathode lamp power supply were identical to the ones described in a previous section (76). The reference lamp power supply (which drove a Beckman type 96280 H_2 lamp as described and utilized by Donnelly) was identical to the hollow-cathode lamp power supply except that the sensing resistor (R_{sense}) was changed from 100 to 10 ohms and a 25 watt light bulb was used as a load resistor (R_L). (A 2.5 volt transformer was also added to power the lamp heater contained inside the Beckman H_2 lamp.)

In order to properly evaluate the stability of the BECS, a test was made to show the system's ability to measure a constant simulated absorbance signal over a reasonable time period. After the reference and sample lamps were balanced to equal intensities, an absorbance was simulated by decreasing the current flowing through the sample lamp. The resulting output from the BECS was digitized by the V-F converter and counted on a scaler. A programmable crystal-controlled timer attached to the scaler allowed this output signal to be counted for a fixed time period. The output of the BECS was counted and recorded at



SW	OPEN	CLOSED
1	VOLTAGE INPUT	CURRENT INPUT
2	AMP GAIN =11	AMP GAIN =1
3	INVERT	NON INVERT
4	NON INVERT	INVERT

Figure 21. The circuit diagram for the input amplifier. The LED is a level indicator which is set to flicker below the BECS integrator overload point.

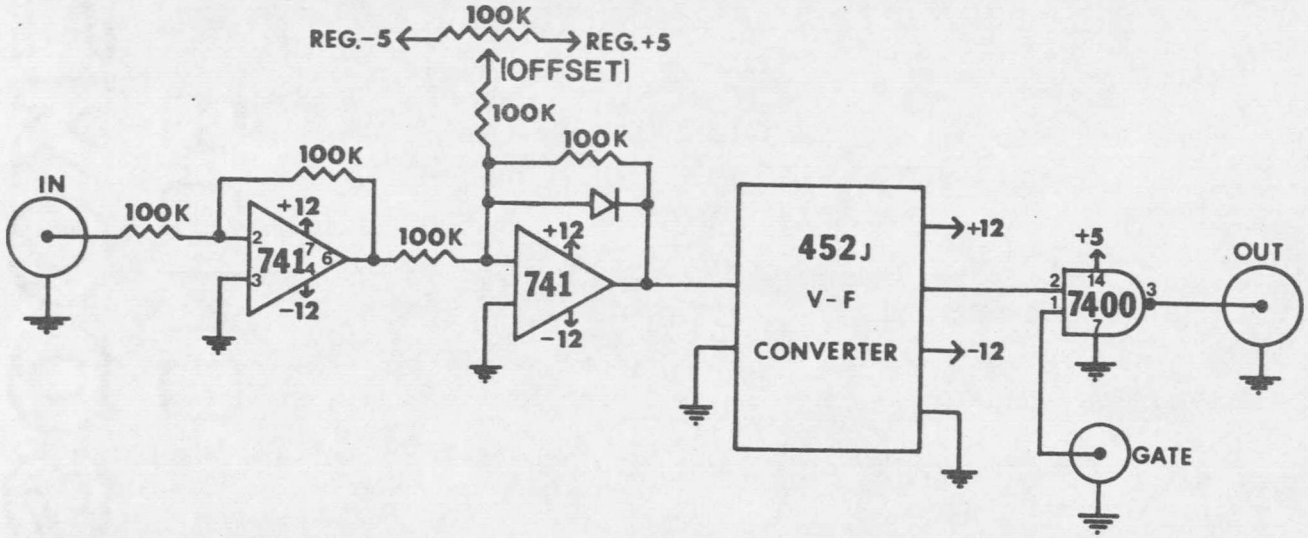


Figure 22. The circuit diagram for the voltage to frequency converter.

40 sec intervals. Results of this test are plotted in Figure 23. Three hundred and sixty samples were taken; 72 points were plotted by averaging groups of five samples. This test shows a larger than expected drift of the BECS output over a four-hour time period (2.45% relative standard deviation). The reference and sample lamps were suspected to be the major cause of this drift and similar stability tests on their output as seen by the P-M tube were made. For these tests the P-M tube signal was fed through the input amplifier to the V-F converter and was likewise counted by the scaler with the attached programmable timer. The lamps were allowed only a three minute warm up prior to sampling their output intensities. Results of this data are also plotted on Figure 23. Observations of this figure reveal, even after a one hour warm up, the intensities of both lamps drift while operating under constant current regulation. Differences in the rates of drift for both lamps partially account for the behavior of the BECS output. To prove this statement, non-drifting lamp intensity signals were needed. These signals were simulated electronically by the summing amplifier diagrammed in Figure 24. The output of this amplifier was fed directly to the input of the BECS. The BECS output was digitized, counted and recorded as before. Results of this data showed a relative standard deviation of 0.59% over a four-hour period. Apparently the weakest link of the system is long term lamp drift. We

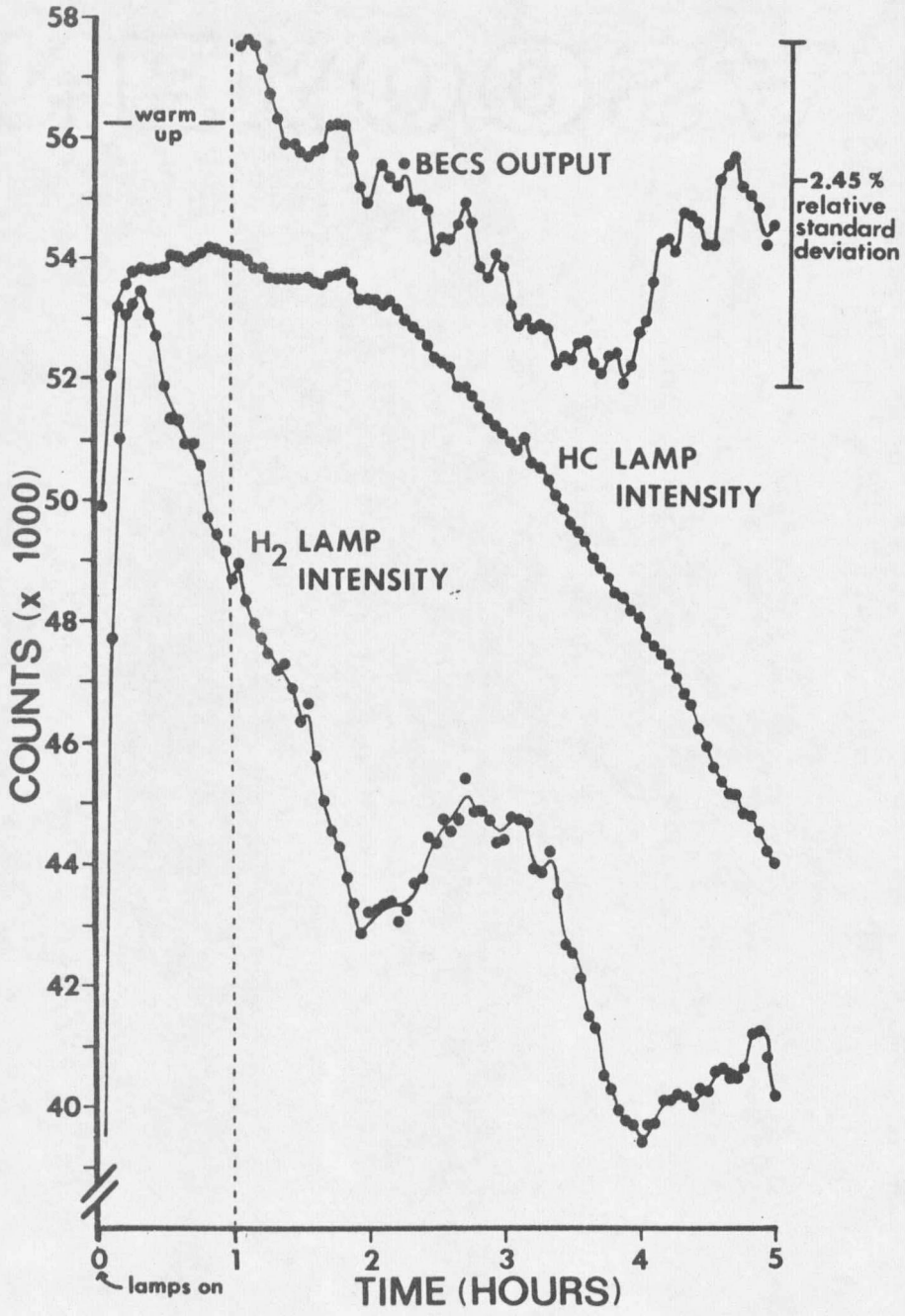


Figure 23. Plotted data for the system's ability to measure a constant simulated absorbance and data for lamp intensity drifts.

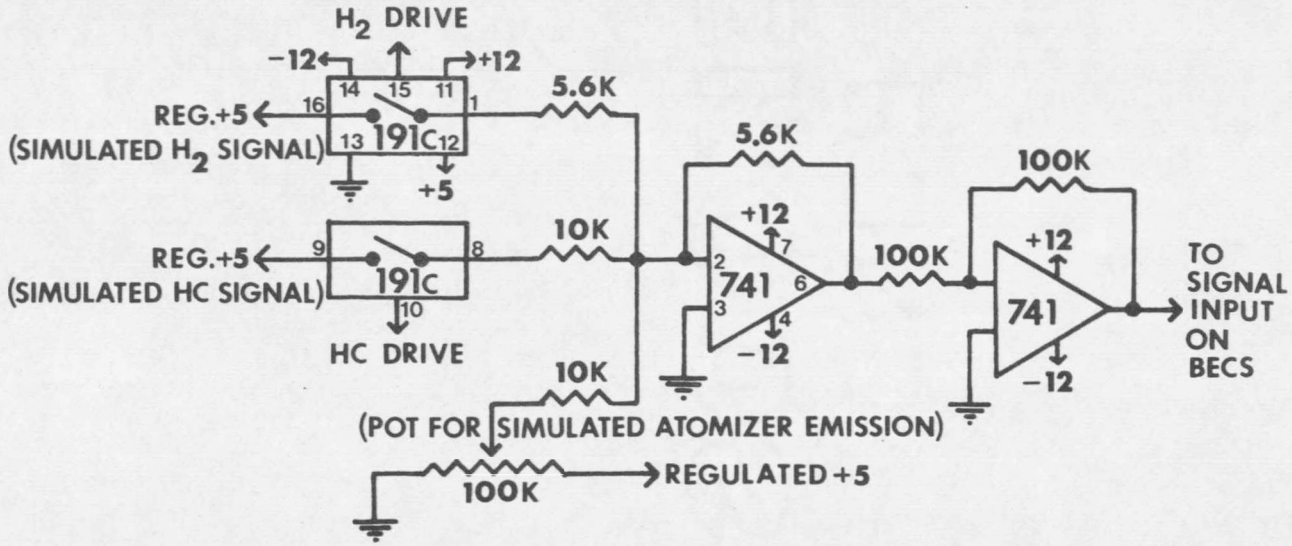


Figure 24. The circuit used to generate simulated sample container emission and lamp intensities.

are currently exploring addition of a reference beam system which will monitor and correct for long term lamp drift.

The system was next tested for its broad band emission correction abilities. Unfortunately, at the time of this experiment, the atomizer had recently been rebuilt and was contaminated with elements which require higher atomization temperatures (such as Cu, Al, Fe, and Ni). However, the atomizer was free of Pb, which requires a lower atomization temperature (1800°C - 1900°C). This lower temperature produces an emission signal of only 1-2% of the sample signal (HC lamp intensity). A larger atomizer emission was simulated by increasing the idle current of the reference lamp. This had the same effect at the P-M tube as increasing background due to higher atomization temperatures. Lead standards were analyzed and the results of this test showed good reproducibility (maximum relative standard deviation of 5.6%) and good linearity at very low concentrations (1 to 3 x 10^{-10} grams of Pb) with an effective atomizer emission of 12% of the sample signal.

The system's ability to correct for broad band absorption was tested as three different magnitudes of broad band absorption. KBr was used for matrix material to decrease the intensity of the reference lamp. This material caused nonconsistent decreases of the reference lamp intensity at equal concentrations (deviating as much as ±40%). Approximately 10^4 to 10^5 times more KBr than analyte was used. In each

of these three tests graphs were made containing two linear plots calculated with a linear regression program on a Hewlett Packard 55 calculator. One plot consisted of samples containing only analyte (Pb) while the other was a plot of samples containing both Pb and KBr. The difference between the two linear plots on each of the three graphs is a measure of the system's ability to correct for broad band absorption. The three different magnitudes of broad band absorption were approximately 12%, 55% and 63% decreases in reference lamp intensities. The maximum deviations of the Pb and KBr plot from the Pb only plot were found be be 2.4%, 0.9% and 2.2%, respectively. The results of the last of these tests is plotted in Figure 25.

3.3.4 Conclusion

The background emission correction system (BECS) has been shown to be quite stable (0.59% relative standard deviation over a four-hour time period) and able to efficiently correct for both broad band emission and absorption.

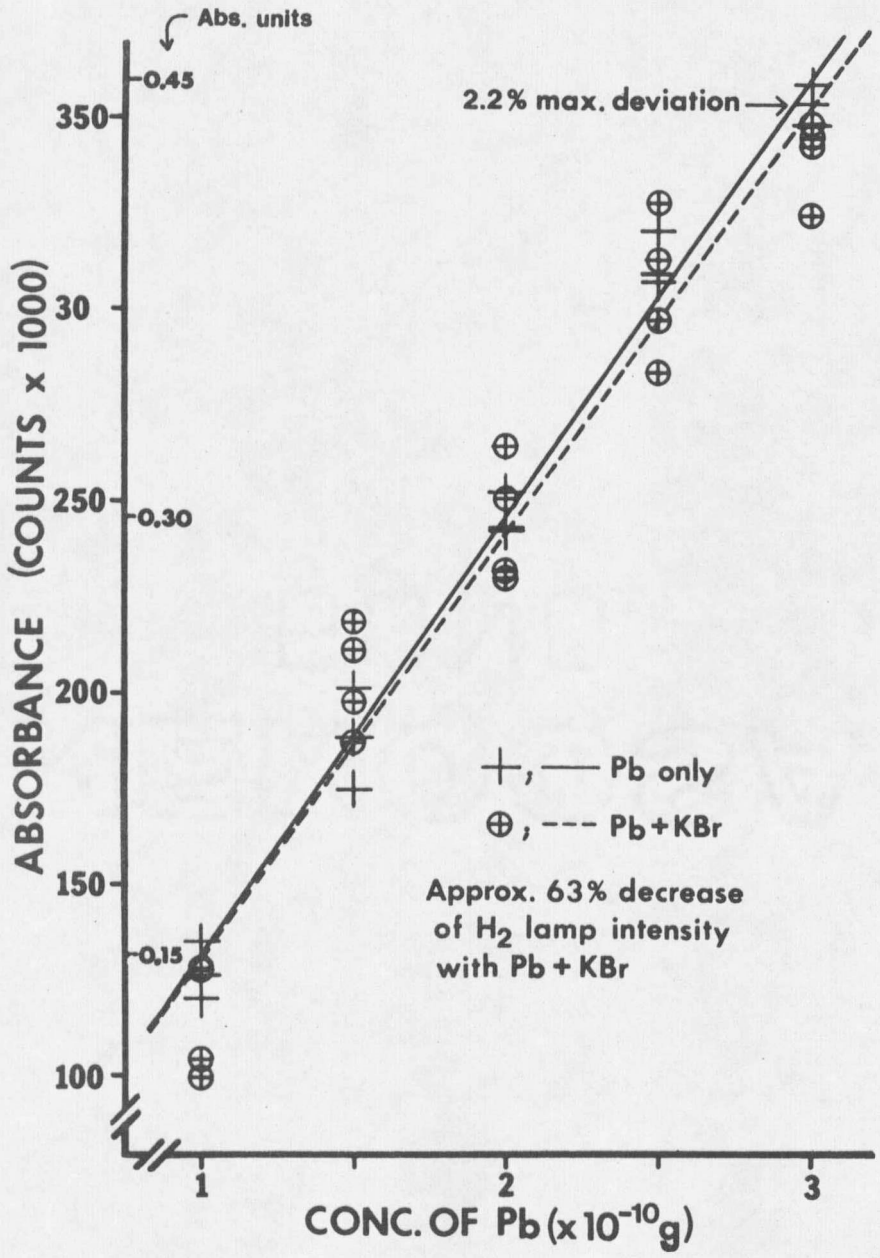


Figure 25. Plotted data for the system's ability to correct for broad band absorption using 90 x 10^{-6} grams of KBr.

CHAPTER 4

Optimization of the Constant Temperature Furnace

4.1 Introduction

Internal graphite part dimensions affect the overall temperature profile. Since the furnace is heated by resistive heating, changing the internal part size changes its resistance, thus changing its power dissipation. Thermal conduction of these parts can also be a factor in producing the overall temperature profile.

The work described in this chapter relates the effects of structural design changes on temperature profiles and the effects of some operational parameters on sample signals. All work is aimed at optimization of the constant temperature furnace as an analytical tool for atomic absorption.

4.2 General Experimental

4.2.1 Electrical

The overall system used was identical to the one described in the previous chapter (54) abbreviated BECS. Sample signal traces were compared to each other by use of the sample insertion marker diagramed in Figure 26. This module was connected between the BECS outputs and the strip chart recorders. The reference signal was monitored by attaching a wire to the 741 operational amplifier following the sample

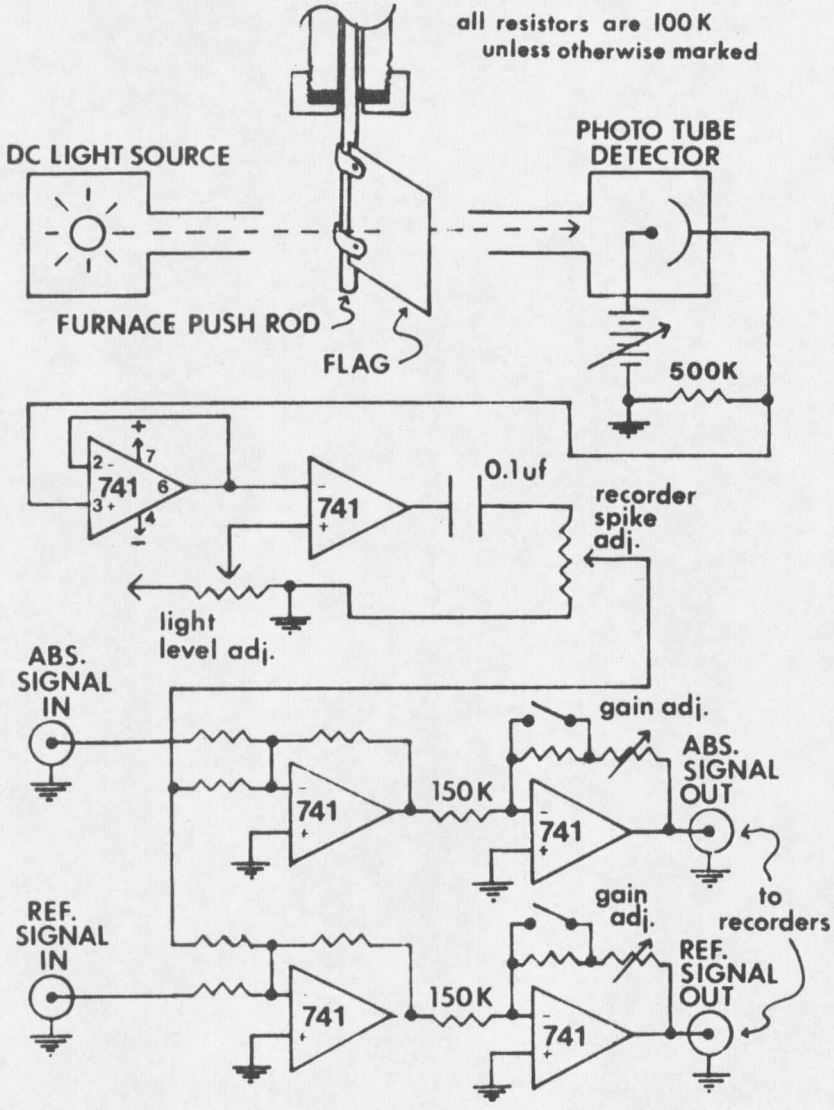


Figure 26. Circuit diagram of the sample insertion marker. The flag on the furnace's pushrod blocks light from the DC light source causing a momentary voltage to be summed with both the absorbance and reference signals. This results in the appearance of a small mark on the strip chart recorder, signaling the completion of the sample introduction.

hold circuit SH_1 inside the BECS. The flag attached to the pushrod of the atomizer was set to block light coming from the DC light source 5 mm before the pedestal mates with the constriction at the top of the side tube in the furnace. This results in the appearance of a small mark on the strip chart recorder tracing as the pedestal seats with the cup chamber.

4.2.2 Reagents and Materials

All chemicals used were of analytical grade. Distilled deionized water was used for making all solutions. Pb standards were prepared by dissolving Pb metal in distilled nitric acid. A 3.500×10^{-4} g/l Pb stock solution was prepared by appropriate dilution. An 11.000 g/l stock solution of #571 NBS orchard leaves was prepared by digestion in distilled nitric acid. Orchard leaf samples were pipetted off the top of the solution as a small residue remained undissolved. A 1% NaCl stock solution was also prepared.

4.3 Experiments, Results and Discussion

4.3.1 Effects of Structural Changes on Temperature

Internal graphite parts of the three phase furnace shown in Figure 7 have typically been constructed from Poco graphite AXF5Q rod stock with the following dimensions: heater tube 9.53 mm O.D. X 7.94 mm I.D.; side tube 12.70 mm O.D. X 10.26 mm I.D.; end posts 9.53 mm O.D. X

6.35 mm I.D. These sizes were originally chosen for reasons of ease of construction, considering rod stock available and mechanical constraints.

Several slightly varying sizes of these internal parts were constructed and systematically substituted one at a time into the standard size system just described. Overall heater tube temperature profiles of each modified system were measured in order to determine the optimum system.

An optical pyrometer was used to determine the temperature profiles inside the furnace. These measurements were taken by focusing through quartz plates (located in the lens caps) onto different shaped graphite markers placed along the length of the heater tube. Temperature profiles up the side tube were similarly taken by replacing the pushrod cap with a quartz plate. The markers inside the furnace were made small enough to have a minimal effect on the actual temperature profile. Temperature differences of about 10°C could be differentiated by this method.

Comparison of results was difficult because of the deterioration of the graphite heater tube as operating time increased. Most of this deterioration is caused by the reaction of graphite with trace amounts of oxygen present in the atomizer. Deteriorated heater tubes weigh less, have smaller cross-sectional areas, draw less current at the same

voltages and thus dissipate less power, lowering the overall temperature profile. The amount of temperature lowering due to deterioration was estimated by weighing the heater tube prior to operating the furnace with each new part substitution. With this information the temperature profiles of each system were corrected to one with an undeteriorated heater tube by use of a temperature versus heater tube weight curve. This curve was constructed by measuring the average temperature of several heater tubes in varying degrees of deterioration at equal furnace voltage settings. The temperature versus heater tube weight curve is quite linear for heater tubes of the same initial dimensions.

The resulting heater tube weight corrected temperature profile curves for each part-substituted system at a furnace setting of 7.0 volts per leg is shown in Figure 27. (Other voltage settings show similar temperature profiles.) Note that all curves show a very hot center temperature compared to the ends of the heater tube. This is due to the increased current flow through the center "tee" section at equal leg voltage settings in three phase powered furnaces (77). The more uniform temperature profile shown in Figure 5 was achieved by dropping the side tube voltage to about half the value of the other two legs. Curve A depicts the resulting temperature profile of the standard size graphite parts system having the dimensions previously

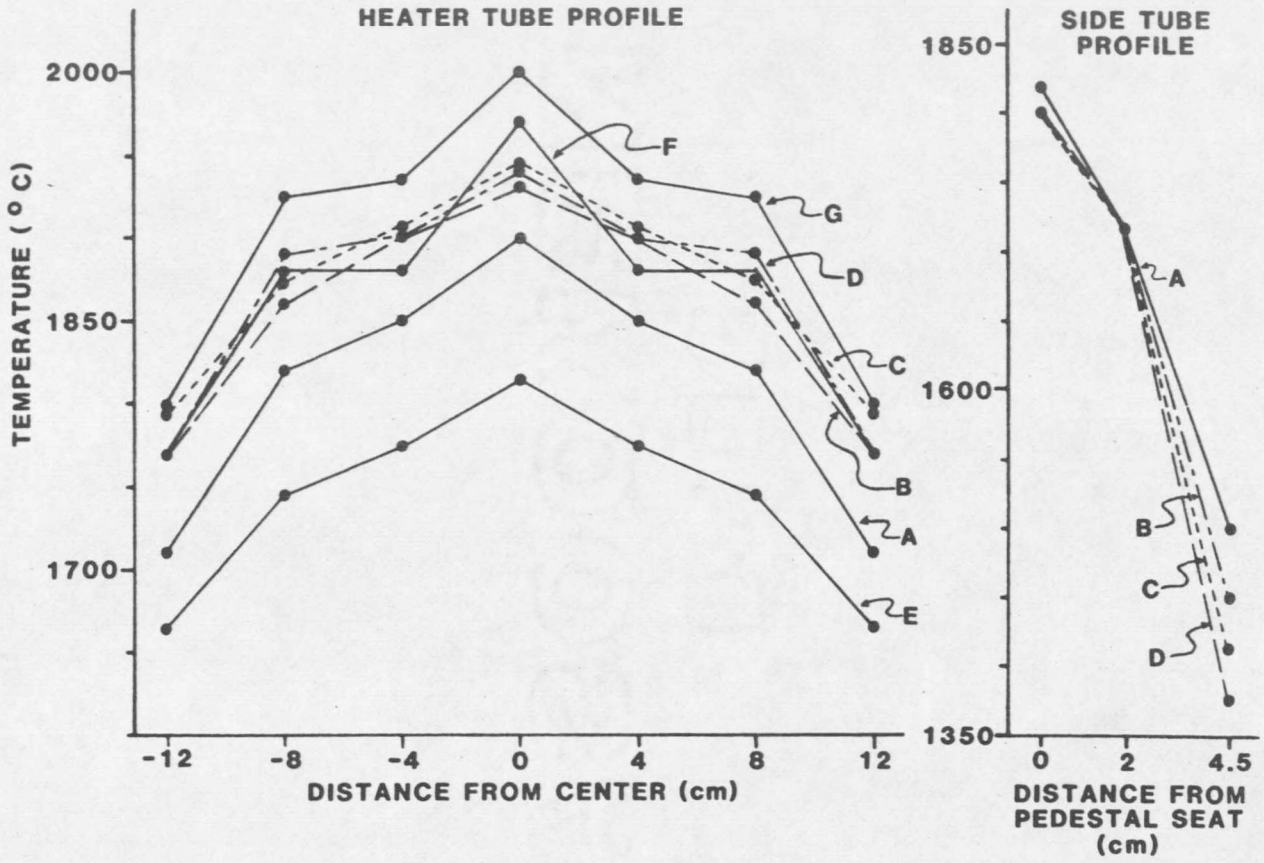


Figure 27. Effects of internal graphite part changes on temperature profiles inside a three phase furnace operating at 7.0 volts per leg. Use of standard sized parts results in Curve A. Curves B, C and D result from the substitution of increasingly thicker side tubes. Curves E and F result from the use of thinner and thicker end posts, respectively. Substitution of a thicker heater tube produces the temperature profile indicated by Curve G.

described. The side tube substitutions used to generate curves B, C and D had progressively increasing cross sectional areas. The dimensions of these side tubes were 12.70 mm O.D. X 9.80 mm I.D.; 12.70 mm O.D. X 9.58 mm I.D.; and 15.88 mm O.D. X 10.26 I.D., respectively. All three raise the overall temperature profile of the heater tube, probably due to increased electrical conduction and less power being dissipated across the side tubes themselves. Curve C has a slightly greater temperature profile than curve B. This is due to the larger cross sectional area of the side tube. However, the side tube used to generate curve D, with its even larger cross sectional area, appears to slightly decrease the overall temperature profile. Continually increasing the cross sectional area of the side tube results in decreasing the temperature profile because thermal conduction away from the heater tube becomes significant. The temperature profile down the side tube for these three side tube substitutions shows this cooling effect. The thickest side tube (curve D) shows the largest temperature change down the side tube. This is a desirable trait in order to minimize premature atomization of samples upon insertion. Increasing or decreasing the size of the cup chamber at the top of the side tube shows little effect on overall temperature profiles. Thus, it is better to manufacture cup chambers as thick as possible since thin cup chambers tend to burn out rapidly due to close proximity to samples and

sample cups containing trace amounts of oxygen. A thick cup chamber also has the advantage of minimizing temperature decreases as samples are inserted, resulting in a more rapid atomization as discussed by Marinkovic et al. (49). Curves E and F resulted from different sized end posts having the dimensions 8.43 mm O.D. X 6.35 mm I.D. and 11.11 mm O.D. X 6.35 mm I.D., respectively. The lower temperature profile generated with use of the thinner end posts results from decreased electrical conduction to the heater tube. The thinner end posts dissipate enough power themselves that they expand significantly, pushing and bending the heater tube away from the optical path. Use of the thicker end posts, depicted by curve F, greatly raises the overall temperature profile by increasing the electrical conduction to the heater tubes and by dissipating less power themselves. Although larger end posts were not tried, it is suspected that increasing the size of the end posts too much will cause the temperature of the heater tube ends to decrease from thermal conduction. Curve G results from the use of a thicker heater tube. The dimensions of the heater tube used to generate this curve were 9.53 mm O.D. X 7.14 mm I.D. The temperature profile of this tube is much higher than the standard tube solely due to its decreased electrical resistance. This tube draws much more current at the same voltage setting than its thinner counterpart and thus dissipates more power.

In conclusion, the optimum sized graphite parts to use in this three phase furnace would be the thicker end posts, a standard size heater tube, and the thicker side tube used to generate curve C constructed with a thick cup chamber. A thicker heater tube is not recommended as excessively large transformers would be required to handle the resulting high currents. Manufacture of the thicker side tube should be done by increasing the outside diameter rather than decreasing the inside. This is because it was found that side tube contamination occurs as a result of the sample pedestal physically contacting the inside of the side tube. Side tube contamination was a problem which plagued earlier furnace models. Contamination on the pedestal and sample cup would be transferred to the side tube wall and back again randomly as samples were inserted. This caused increased analyte signals in some cases and decreased analyte signals in others. Enlarging the inside diameter of the side tube along with the addition of a pushrod guide to stop pedestal wobble eliminated this problem.

4.3.2 Effects of Argon Flow and Sample Insertion Rate

Figure 28 shows the effect of temperature on absorbance for two different argon flow rates and two different sample pedestals. Both peak height and peak area are shown for the ground state 283.3 nm Pb line. 2.8 ng of Pb was used to produce the absorbances of all curves shown in the figure. All points shown on curves are mean values

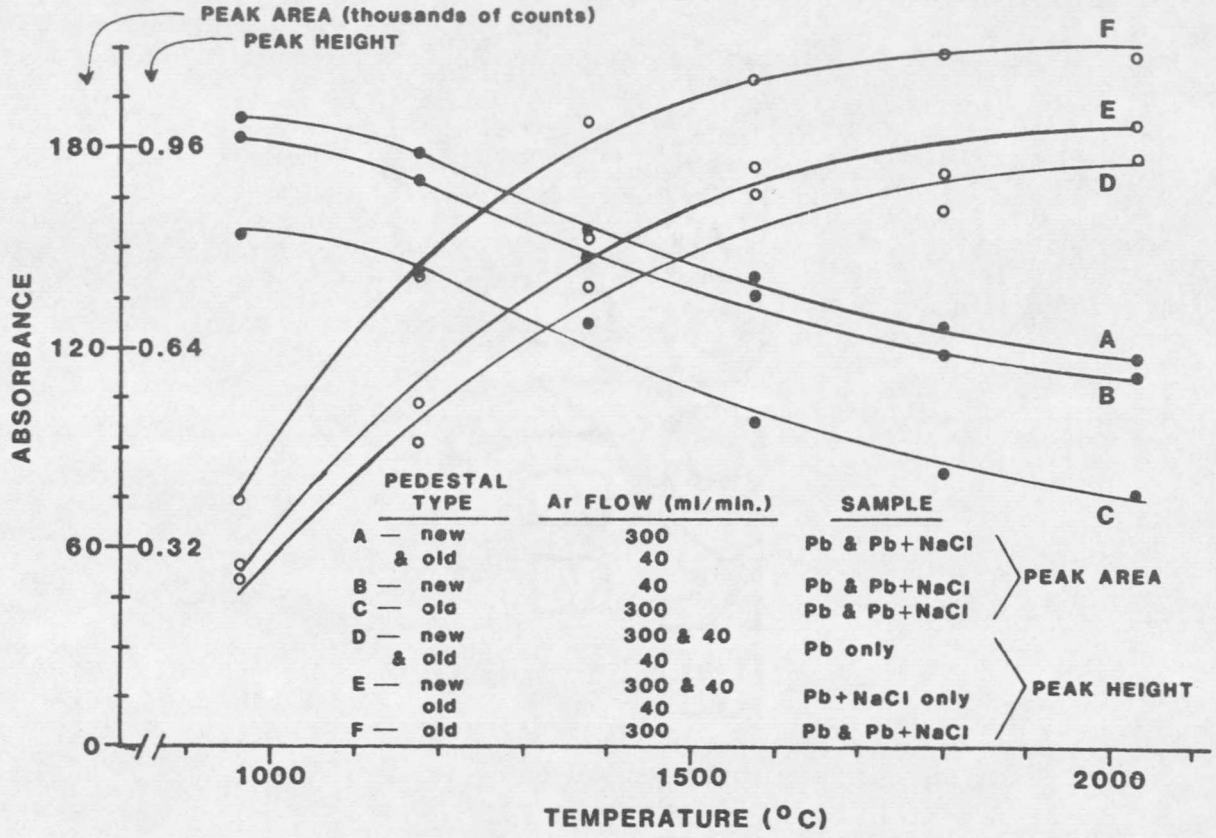


Figure 28. Temperature versus Pb absorbance curves for both peak area and peak height measurements taken under varying conditions of argon flow rate and sample pedestal conditions. All points plotted are average values resulting from 2.8 ng of Pb at a wavelength of 283.3 nm. Addition of 40,000 ng of NaCl affects only the peak height absorbances under the operating conditions used to generate curve D.

calculated from analysis of five to ten samples each. All peak area curves show a decreasing absorbance as the temperature increases. This is caused by decreasing analyte residence times in the heater tube as increased temperatures increase the overall diffusion rate. All peak height curves show larger absorbances as the temperature increases. This is due to faster vaporization and atomization rates at higher temperatures. Addition of 40,000 ng of NaCl did not affect any of the peak area absorbances. The physical condition of the pedestal does affect both peak area and peak height absorbances. Pedestals are originally made to mate tightly with the constriction at the top of the side tube. If this seal is tight, then sample vapor coming out of the crucible resting on the pedestal can only flow into the heater tube. However, pedestals tend to deteriorate rapidly because of their close proximity to the sample and the constant exposure to atmospheric oxygen when the sample port window is opened. Argon is introduced into the furnace slightly above the sample port window which flows out of the sample port when opened. This helps reduce deterioration, but even minor deterioration causes the mating face of the pedestal to become inefficient in sealing. As a consequence, after a short amount of use on a new pedestal, argon flowing past this deteriorated seal can affect the residence time of the analyte in the optical path. Curve A in Figure 28 results from the use of a new pedestal at an argon flow rate

of 300 ml/min and the use of an old pedestal at 40 ml/min. These curves are statistically the same for both conditions because the new pedestal effectively seals and stops the majority of the argon flow. The use of an old pedestal at 300 ml/min, as shown by curve C, results in much lower peak area absorbances. This is due to argon flowing past the deteriorated pedestal seal sweeping the analyte out of the heater tube, reducing analyte residence time. Curve B results from the use of a new pedestal at 40 ml/min. These conditions would be expected to produce a curve that matches curve A. However, the lower absorbances actually observed probably result from back diffusion of some of the analyte vapor past the pedestal seal into the side tube, removing them from the optical path. Argon flow at 40 ml/min is stopped well enough to allow this back diffusion process to occur using a new pedestal. Evidence of this theory comes from the observation that if the pedestal seal is cracked open after the maximum peak height has passed, an increase in absorbance is observed which results in a total peak area absorbance equal to that depicted by curve A. Addition of 40,000 ng of NaCl does affect peak height. Curve D results from a new pedestal used at an argon flow rate of 300 ml/min and 40 ml/min and an old pedestal at 40 ml/min. Addition of chloride with these same conditions produces larger peak height absorbances as shown by curve E. This increase in peak height absorbance is probably due to PbCl gas carrying the Pb out

into the optical path faster than Pb would alone. This early Pb appearance time, which can cause matrix interferences with small pulsed type atomizers (22,78), is easily seen on the strip chart recorder tracings diagrammed in Figure 29. Curve F in Figure 27 resulted from an old pedestal used at an argon flow rate of 300 ml/min. The peak height absorbances are much higher due to argon flowing past the pedestal seal driving the analyte vapor into the optical path faster than the normal diffusion rate. Addition of NaCl, as would be expected, has no effect under these conditions.

Sample insertion rates can also affect peak area and peak height absorbances. Samples are inserted into the furnace by placing them through the sample port window and pushing the pedestal up until contact is made with the cup chamber. If the pedestal is pushed up too slowly, premature vaporization and atomization can take place. Atoms can be trapped inside the side tube, consequently not entering the optical path for detection. This problem becomes worse at higher temperatures, especially for the more volatile elements. Proper design of the side tube, as previously discussed, can help alleviate this problem. Results of studies on this effect are shown in Figures 30 and 31. The fast insertion rate required approximately 1/3 sec while the slow insertion rate required approximately 3 sec to complete. Two different argon flow rates, 240 ml/min and 40 ml/min, were also

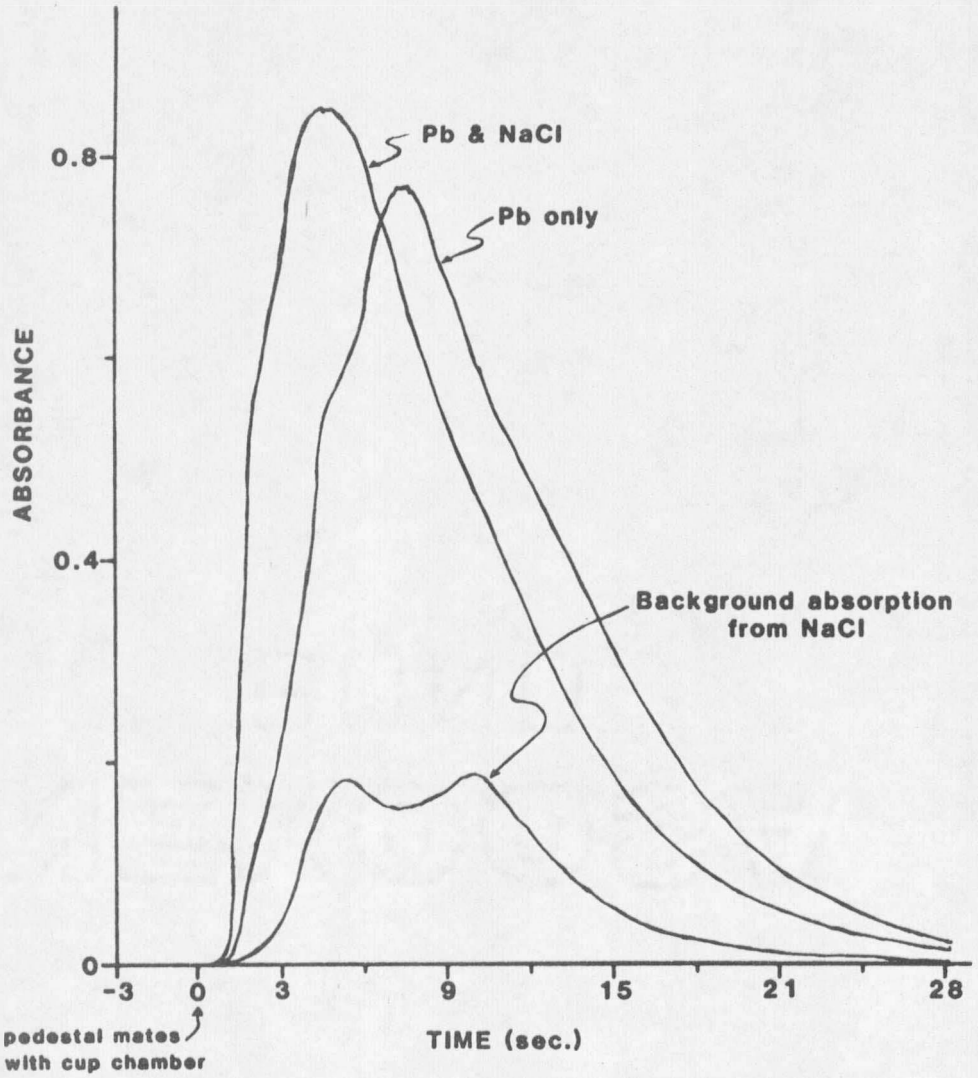


Figure 29. Diagram of strip chart recorder tracings showing the effect of 40,000 ng of NaCl on a 2.8 ng Pb signal at 1175°C in a three phase furnace. NaCl causes the Pb signal to appear earlier, increasing the peak height while the peak area remains the same.

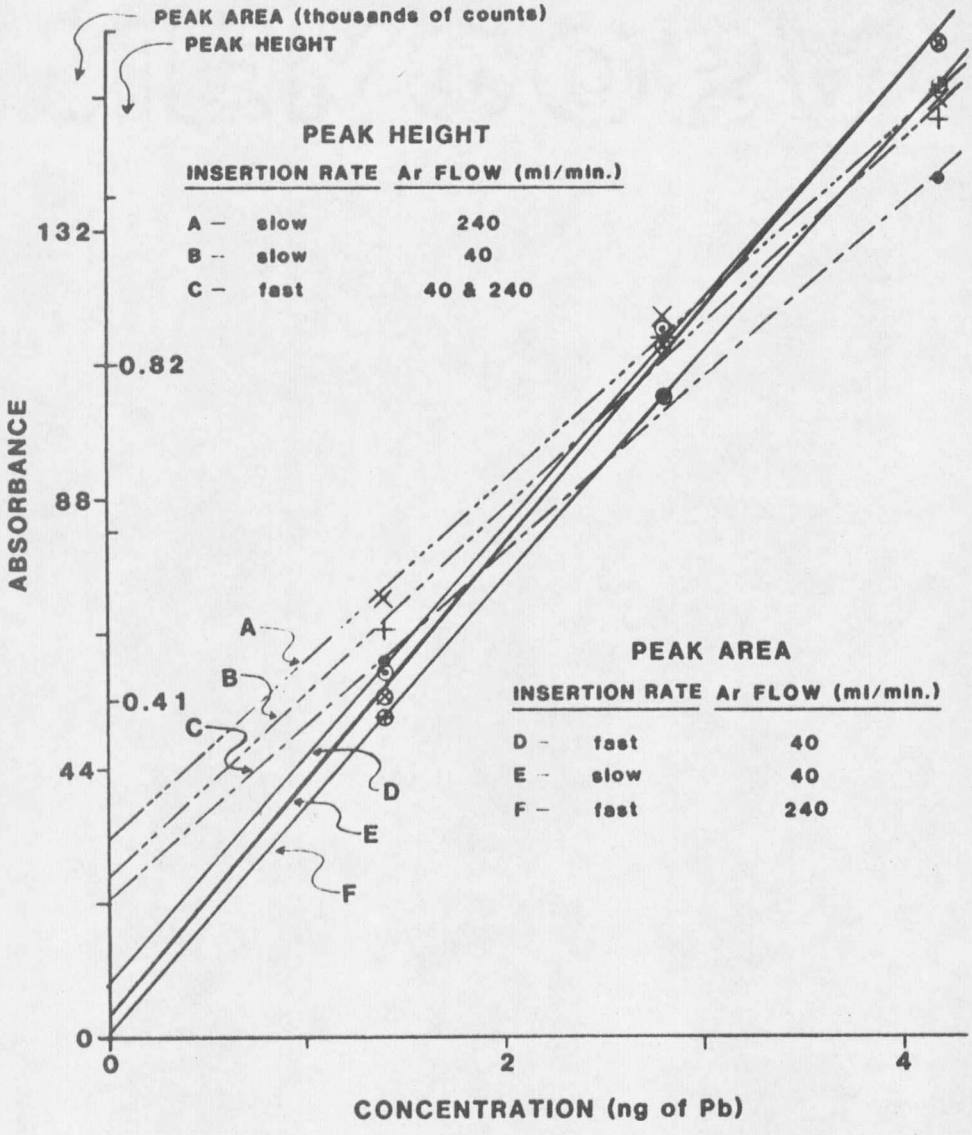


Figure 30. Pb absorbance versus concentration curves measured under varying conditions of sample insertion rate and argon flow. Both peak height and peak area measurements at the 283.3 nm Pb line with an average furnace temperature of 1750°C are shown.

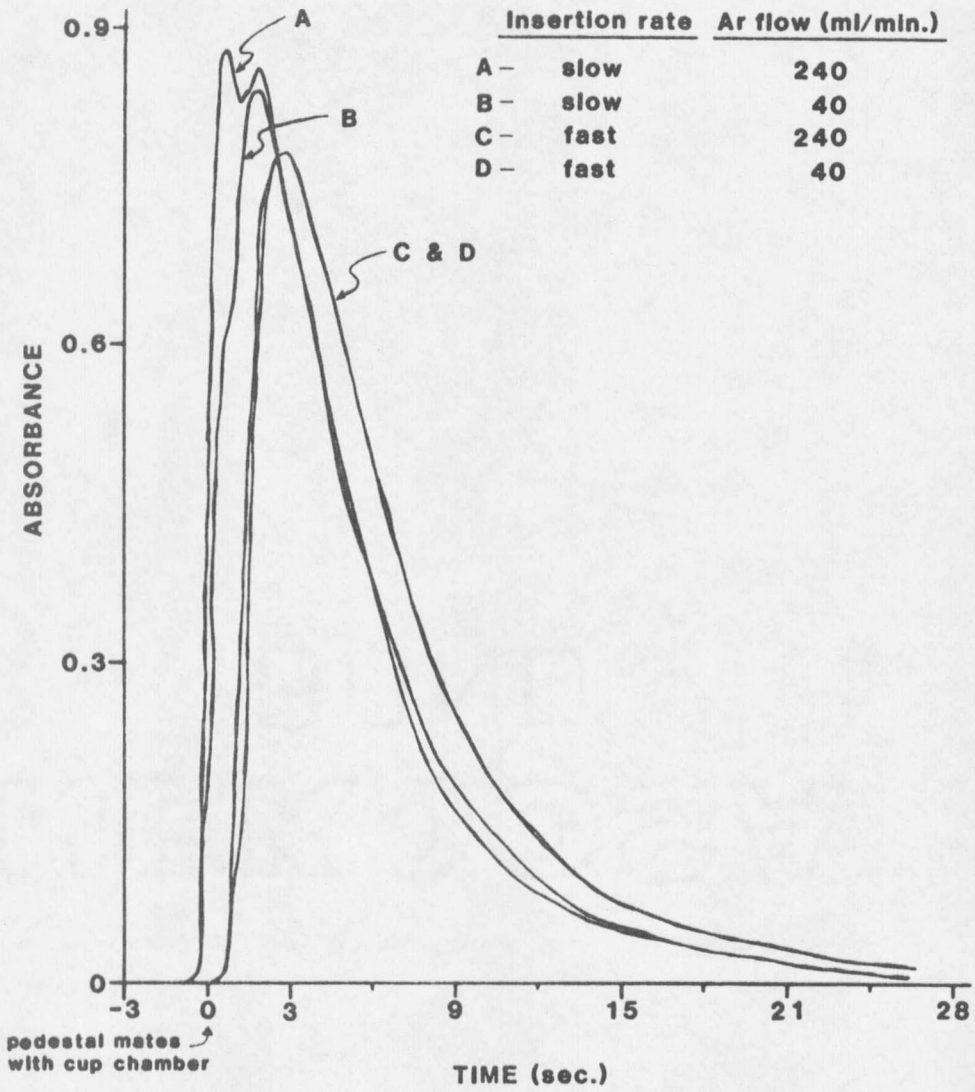


Figure 31. Diagram of strip chart recorder tracings showing premature atomization for slowly inserted samples. All tracings resulted from 2.8 ng of Pb measured at the 283.3 nm line inserted into a three phase furnace operating at 1750°C.

included with this study. Figure 30 shows the effect of these parameters on standard absorbance versus concentration plots for both peak height and peak area. All linear plots were calculated with a linear regression program on a Hewlett-Packard 55 calculator. Extracted NBS orchard leaf samples were also analyzed under each condition and the resulting Pb concentrations calculated with the same linear regression program. The peak area plot for the fast insertion rate at an argon flow of 40 ml/min has a higher absorbance than the fast insertion rate at 240 ml/min. This is due to a slight deterioration of the pedestal at the time of this experiment. Peak height plots of the fast insertion at an argon flow of 240 ml/min and the fast insertion at 40 ml/min are statistically identical and are shown as one plot. This is expected from the temperature versus absorbance data previously discussed. Increased absorbances for peak height plots at slow insertion rates are caused by premature vaporization and atomization. The analyte vapor prematurely produced is probably kept slightly ahead of the advancing pedestal by the high argon flow rate of 240 ml/min creating the large observed peak height. However, at only 40 ml/min, argon flow is slow enough that sample vapor probably cannot keep up with the advancing pedestal. This results in trapping some of the sample vapor in the side tube lowering the peak height. Since the pedestal is slightly deteriorated, most of the

trapped vapor is ultimately pushed past the seal into the optical path adding to the peak area absorbance. Some of the trapped analyte vapor probably finds its way through the porous graphite walls and is lost. The fraction lost in this manner appears to become significant at lower sample concentrations. This statement results from the observation that the mean peak area absorbance at 40 ml/min for 1.4 ng of Pb is statistically lower (at the 95% confidence level) than the 240 ml/min value. Premature vaporization and atomization at slow insertion rates can be seen on the strip chart recorder traces diagrammed in Figure 31. Peak area data for the slow insertion rate at 240 ml/min is very erratic and not very linear. Use of linear regression to graph this data produces a misleading plot and is thus not shown in Figure 30. The values of Pb analysis on NBS orchard leaves for the following insertion and argon flow rates: fast at 40 ml/min, fast at 240 ml/min, slow at 40 ml/min, and slow at 240 ml/min are 44 μg/g, 52 μg/g, 41 μg/g, and 26 μg/g for peak areas and 42 μg/g, 50 μg/g, 34 μg/g, and 37 μg/g for peak heights, respectively. The Pb values found for the fast insertion rate at an argon flow rate of 40 ml/min for both peak area and peak height agree quite well with the 44 μg/g Pb value listed by NBS. The other operating conditions result in larger deviations. The higher argon flow rates were found to cause average relative sample standard deviations over twice as large as that of

slower flow rates.

The conclusion of these operating parameter studies is that optimum results can be attained by using low argon flow rates combined with fast sample insertion. However, slowing argon flow too much can lead to rapid deterioration of internal graphite parts due to back diffusion of atmospheric oxygen. A stop flow system during sample insertion and atomization, as implemented on some commercial atomizers, also may not be a good method due to back diffusion of sample vapor down the side tube. Peak area absorbances should be used as they are much more reliable; matrix materials seem to have no significant effect on their values as compared to peak height measurements where matrix materials do change peak height values.

4.3.3 Three Phase Versus Single Phase Furnaces

Questions have arisen during the design and implementaion of three phase furnaces as to whether they are significantly better than single phase furnaces so as to necessitate the extra expense and construction complications. There is no doubt that three phase furnaces have a much more uniform temperature profile than single phase furnaces. Whether this temperature profile difference really affects sample analysis is a question which has been previously unanswered. An experiment was performed to compare the two systems. In order to eliminate possible effects from movement of two completely different furnaces on and off

the optical rail, the single phase temperature profile was simulated in the three phase furnace. This simulation was done by reducing the current flow through the side tube by use of an external resistor and by attaching massive graphite parts to the end of the heater tube. This simulation was only partially successful at attaining the actual temperature profile of a real single phase furnace. The simulated temperature profile used for this study is shown in Figure 5. Standard Pb concentration versus absorbance curves for each system were statistically the same for both peak height and peak area absorbances. Pb analysis on NBS orchard leaf extracts were likewise identical.

The conclusion is that for routine analysis, a single phase furnace would perform equally as well as the more complicated three phase furnace. However, for special applications where uniform temperature profiles would be helpful, such as vapor pressure measurements (51), a three phase furnace would be worth the expense. In the past, single phase furnaces have often had the problem of attaining very high temperatures. Three phase powering delivers much more power per unit time to the heater tube. Very high temperatures are thus more easily attainable with three phase furnaces. Although not found in this study, possibly because of the inability to correctly simulate a single phase furnace temperature profile, variation in heater tube temperature as a sample passes down the tube might possibly

cause interferences for samples with complex matrices. If true, then a three phase powered furnace will prove a worthwhile investment.

CHAPTER 5

Conclusions and Suggestions for Further Work

Design changes discussed in this thesis have improved the overall efficiency and have made the constant temperature furnace (CTF) a much more easily manipulated atomizer than the first early models. Detailed studies of the effects of various operational parameters on the CTF allow trace metal analysis to be performed at optimum furnace conditions. New supporting electronics combined with a modern CTF produce an atomic absorption system capable of accurate analysis of samples difficult to analyze on a normal atomic absorption spectrometer. CTFs freedom from matrix interferences makes them ideal tools for both routine analysis of samples with complicated matrices and research applications. CTFs are versatile. Liquid samples nebulized and dissolved can be introduced directly into the furnace. Solid or liquid samples in graphite crucibles can be prepared 100 samples at a time under appropriate conditions without tieing up the instrument. Particulate matter filtered from air or liquid samples through porous graphite crucibles are inserted directly into the furnace thus eliminating sample preparation and contamination. Broad-band absorption from organic material can ordinarily be reduced to a manageable level by use of graphite crucibles with porous lids.

It is difficult to understand why so many manufacturers of commerical atomic absorption instruments have expended vast amounts of time and money putting modern electronics, optics and computers with an atomizer that does not provide a dependable measure of the analyte present. I anticipate an increase in the utilization of constant temperature furnaces over the next decade as manufacturers strive to develop more accurate atomic absorption spectrometers.

Future studies using the CTFs are endless. Direct analysis of many samples previously impossible to analyze by atomic absorption may now be possible using the CTF. Successful mating of CTFs with gas chromatographs and mass spectrometers may produce an ideal tool for high temperature studies of chemical reactions. Simultaneous measurements of atomic emission and atomic absorption may be possible with a slight modification of the BECS system described in this thesis. Since the furnace emission signal is examined in absence of the reference and atomic line signals inside the BECS, an integration and sample hold circuit for the emission signal alone can be added without disrupting the absorbance computation. This emission signal can be output to a V-F converter and counted on a scaler. By masking off the furnace light portion of the emission signal with the offset control on the V-F converter, both atomic emission and atomic absorption can be monitored. Although the number of excited state atoms at obtainable

furnace temperatures is low for many elements, some elements should have sufficient emissions to make these measurements worthwhile. Simultaneous emission and absorption measurements may not only help widen useable concentration ranges but may prove useful in studying distribution of ground state and excited state atoms under varying conditions.

APPENDIX

A Temperature Controlled Annealing Oven for Glassware

Introduction

Sample crucible contamination can be a serious problem in atomic absorption analysis with a constant temperature furnace. Clean crucibles must be stored in a clean chamber to prevent unwanted contamination. A very good crucible storage chamber can be made from a pyrex petri dish. Small sections of pyrex tubing are cut and attached to the bottom half of the petri dish to hold the individual crucibles. Crucibles can be carried into the field without rearrangment or contamination by taping closed the small gap present between the two halves of the petri dish. Attachment of the tubing sections to the bottom half of the petri dish is difficult. The use of glue has proved unsatisfactory because of its lack of resistance to acid cleaning solutions. Direct use of a torch to seal the tube sections to the petri dish results in cracking. An oven is necessary to preheat the dish prior to application of a hand torch. Muffle furnaces have been used but temperature control and proper annealing of the finished product is difficult. A temperature controlled annealing oven made for glassware is the best solution to this problem.

Annealing depends on two factors: time and temperature (79). As

the temperature increases, the time to relieve strain is decreased. Heating rates in an annealing oven cannot be too rapid or cracking can occur. Cooling rates cannot be too rapid or strains will redevelop. The oven presented here controls the heating rate and the soaking time at a maximum temperature required to properly anneal glassware.

Circuit Description

The circuit diagram for the temperature controlled annealing oven is shown in Figure 32. The two 8 ohm resistors used for heating elements inside the oven are made from No 16 gauge nichrome wire. Current flow through these heating elements is controlled by gating on and off two 2N5445 power triacs via two Motorola MOC3030 IC chips. The MOC3030 is an optically coupled zero crossing triac which allows isolation of AC line voltage from low voltage digital logic. Zero logic applied to pin 2 of the MOC 3030 turns on an internal LED which gates on an internal triac connected between pins 4 and 6 if the applied AC voltage is near zero potential (thus the name zero crossing triac). Once a triac is gated on it continues to conduct until the applied voltage crosses zero. Turning on high power traics using small integrated circuit chips can be difficult because of the fairly large gate currents required. The MOC3030 is rated at a maximum of 100 mA continuous operation. This is not enough to drive a high power triac. However, this IC ship can handle up to 1.2 A of momentary surge current

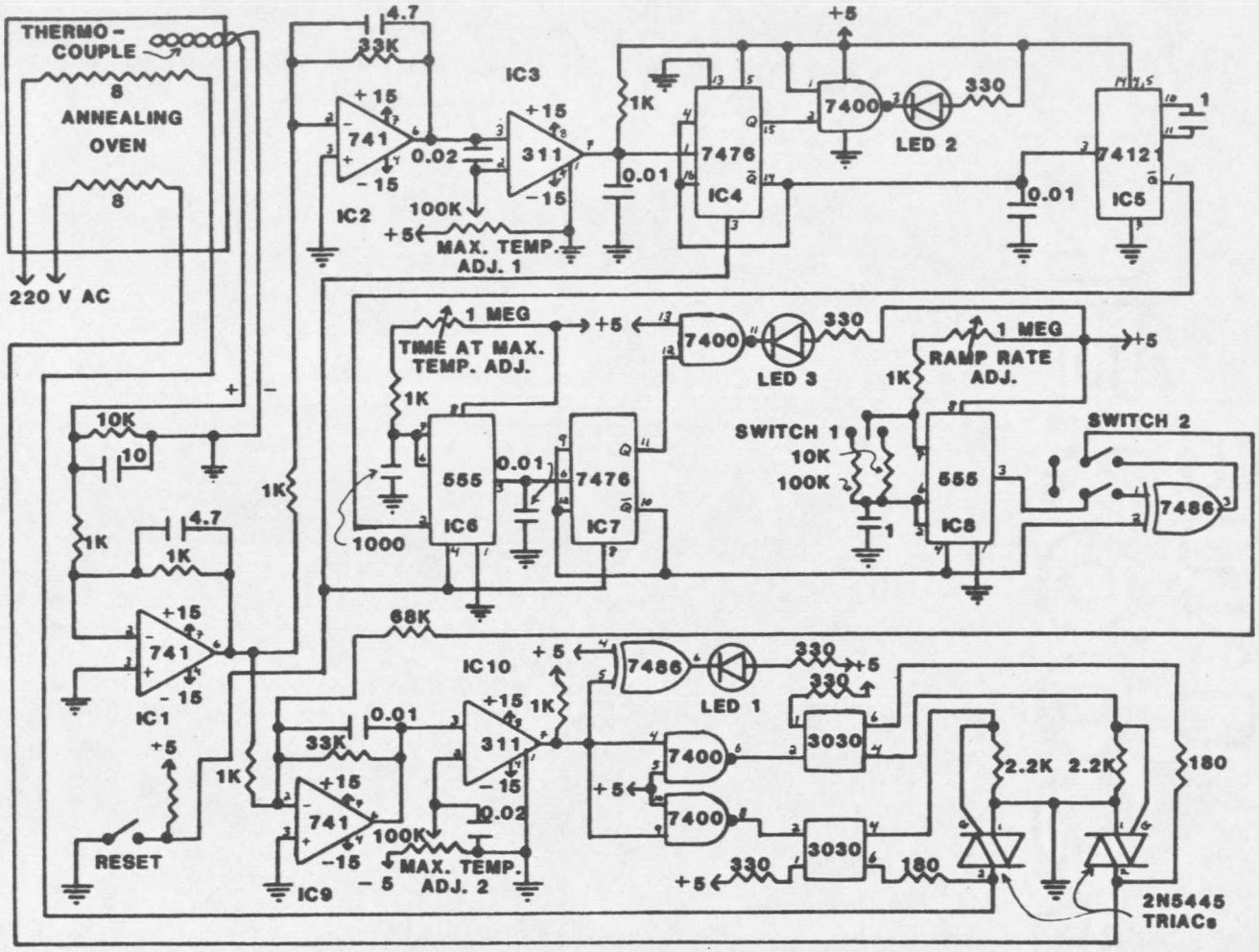


Figure 32. Circuit diagram of the temperature controlled annealing oven. All resistors are in ohms and capacitors are in microfarads.

which is capable of driving even the largest currently available power triacs. Current regulation through the heating elements with the power triacs may be understood by following the AC voltage changes starting from the time the AC voltage crosses zero. If the triac inside the MOC3030 is gated on, current will flow through the 180 ohm and 2.2 K ohm resistors as the voltage increases. The potential at the power triac gate likewise increases and current flows into the gate since the resistance from the gate through the triac to ground is low. When the current flow into the gate is sufficient to turn on the power triac, the voltage drop across the triac drops dramatically. Thus, current flow through the MOC3030 triac also drops, protecting the IC chip from excessive power dissipation. Temperature inside the oven can then be controlled by how often the LED-triac couples inside the MOC3030s are turned on with the 7400 NAND gates. These NAND gates are regulated by the comparitor circuit IC 10. IC 10 compares the output of IC 9 with the potential set by the potentiometer labelled MAX TEMP ADJ 2. A more positive potential from IC 9 inhibits oven powering while a more negative potential turns on the LED-triac couple. The output of IC 9 is determined by the summation of the thermocouple signal from IC 1 and the pulses coming from the pulse generator IC 8. Logic one pulses from IC 8 drive the output of IC 9 negative, turning on the oven power. Increasing temperature sensed by the thermocouple drives the output of

IC 9 more positive. The potentiometer in the comparator circuit can thus be adjusted to inhibit oven powering at any desired temperature. The temperature inside the oven can be held at a fairly constant maximum value with this arrangement. ICs 2 through 7 regulate the amount of time the oven is held at this maximum temperature. IC 2 amplifies the thermocouple signal. The comparator circuit IC 3 compares the output of IC 2 with the potential set by the potentiometer labelled MAX. TEMP. ADJ. 1. When the output of IC 2 becomes more positive than this potential the output of IC 3 drops to zero triggering the J-K Flip Flop IC 4. This causes illumination of LED 2 indicating the maximum temperature has been reached; while triggering the monostable IC 5. The short pulse produced from IC 5 is necessary to trigger IC 6 which is wired as a long time period monostable capable of logic one pulses up to 15 minutes long. The length of this monostable controls the time period the oven is held at the maximum temperature. The falling edge of this monostable pulse at the end of the time period triggers IC 7 which stops the pulse generator IC 8. LED 3 is also illuminated indicating the end of the time period at maximum temperature. LED 1 indicates when power is applied to the heating elements. During the heating up of the oven this light flickers at a rate determined by the pulse widths of IC 8. Once the maximum temperature is reached this light comes on periodically as

power is applied to hold the temperature constant. When LED 3 is illuminated LED 1 remains off and the oven starts to cool down until the heating and holding cycle is started over again by momentarily closing the reset button.

The rate at which the oven heats up can be important. Too fast a rate can crack strained glasswork. Too slow a rate can take excessively long time periods to reach the maximum temperature.

Regulating the length of time IC 8 is at logic one changes the length of time the heating elements are powered. The rate of oven heating can thus be changed by varying the logic one pulse widths. Increasing the resistance with the RAMP RATE ADJ. potentiometer speeds up the heating rate. The heating rate can be adjusted for slower rates by inserting the exclusive OR gate with SWITCH 2.

The rate of cooling is not directly controlled by the electrical circuit but is limited by the insulating ability of the oven shell. Controlling the cooling rate in this manner is adequate while greatly simplifying the electrical circuit.

Experimental Results and Discussion

The annealing oven used to test the previously described control circuit was made from an old discarded electric pottery kiln. Burned out heating elements were replaced and the control circuitry was attached with proper heat shielding. An iron-constantan thermocouple

was used and output to a front panel to monitor the oven temperature using a digital millivolt meter. A soaking temperature of 580°C was chosen for annealing the mixed sizes of pyrex glassware typically made and repaired in a general laboratory. Both MAX TEMP. ADJ. potentiometers were adjusted to illuminate LED 1 (controlled by ADJ. 1) when LED 3 first turns off (controlled by ADJ. 2) at 580°C. A soaking time of 13 minutes was established by adjusting the TIME AT MAX. TEMP. ADJ. potentiometer. The soaking time can be measured by observing the time between illumination of LED 2 and LED 3.

The amount of power on state required to achieve a certain heating rate depends a great deal on the insulting ability of the oven. The heating rates decrease as the temperature increases due to heat dissipation. If the heating rate is set while the oven is cool, the oven may not achieve the desired maximum temperature due to this heat dissipation. The heating rate must be set when the oven temperature is near the desired maximum temperature. A heating rate of 10°C/min at 560°C resulted in a 40°C/min rate near room temperature. (This heating rate can be slowed to 20°C/min without adjusting the potentiometer by inserting the 100K ohm resistor instead of the 10K ohm resistor on IC 8 with SWITCH 1. This switch can be used to initially heat up highly strained glasswork.) The overall annealing cycle required approximately 3 hours (1 hr for heating up and 2 hr for cooling off).

Much better control could be achieved by converting to microprocessor control. Proper software programming with temperature feedback could result in a steady heating rate as well as a controlled cooling-off rate not available with the system presented here. The cost of such a system however would be considerably higher.

REFERENCES

1. G. Kirchhoff, Pogg. Annalen 109, 275 (1860).
2. G. Kirchhoff, Phil. Mag. 20, 1 (1860).
3. G. Kirchhoff and R. Bunsen, Phil. Mag. 20, 89 (1860).
4. G. Kirchhoff and R. Bunsen, Phil. Mag. 22, 329 (1861).
5. A. Walsh, Spectrochim. Acta 7, 108 (1955).
6. C. Th. J. Alkemade and J. M. W. Milatz, Appl. Sci. Res. 4b, 289 (1955).
7. C. Th. J. Alkemade and J. M. W. Milatz, J. Opt. Soc. Am. 45, 583 (1955).
8. J. E. Allan, Analyst 83, 466 (1958).
9. D. J. David, Analyst 83, 655 (1958).
10. J. B. Willis, Nature 107, 715 (1965).
11. Y. Talmi, Anal. Chem. 47, 658A (1975).
12. D. Burgess, U. S. Bureau of Mines Bulletin 504 (1962).
13. V. A. Fassel, R. N. Kniseley and A. P. D'Silva, Anal. Chem. 35, 910 (1963).
14. J. B. Willis, "Methods of Biochemical Analysis," Vol. XI, Interscience, New York (1963).
15. S. R. Koityohann and E. E. Pickett, Anal. Chem. 38, 1087 (1966).
16. V. A. Fassel and D. A. Baker, Anal. Chem. 41, 1522 (1969).
17. B. V. L'vov, Eng. Phys. J. S. S. R. 2(2), 44 (1959).

18. R. W. Stone, "The Graphite Furnace as An Atomzation Cell for Atomic Absorption Spectroscopy," Ph.D. Dissertation, Montana State University, Bozeman, Montana (1974).

19. E. Lundberg, "Instrumental Developments in Graphite Furnace Atomic Absorption Spectroscopy with Applications to Direct Determintions of Trace Metal in Solid Samples," Ph.D. Dissertation, University of Umea, Umea, Sweden (1979).

20. S. R. Lawson, "Effect of Furnace Design on Atomic Absorption and Emission Signals in Spectrochemical Analysis," Ph.D. Dissertation, Montana State University, Bozeman, Montana (1981).

21. E. Lundberg and W. Frech, Anal. Chim. Acta 104, 75 (1975).

22. L. Hageman, A. Mubarak and R. Woodriff, Appl. Spectrosc. 33, 226 (1979).

23. L. Hageman, J. A. Nichols. P. Viswandham and R. Woodriff, Anal. Chem. 51, 1406 (1979).

24. B. V. L'vov, Spectrochim. Acta 17, 761 (1961).

25. B. V. L'vov, Spectrochim. Acta 24B, 53 (1969).

26. R. Woodriff and G. Ramelow, Abstracts, Society for Applied Spectrosc., Chicago, Ill., No. 83, June 1966.

27. B. Watne, "Development of a Constant Temperature, Platinum, Atomic Absorption Furnace and its Use in Potassium Vapor Pressure Measurements for MHD," Ph.D. Dissertation, Montana State University, Bozeman, Montana (1977).

28. Poco Graphite Inc., 1601 S. State St., Decatur, Texas, USA 76234.

29. Union Carbide Corp., Carbon Products Division, 270 Park Ave., New York, N.Y., USA 10017.

30. G. Ramelow, "Atomic Absorption Spectrosopy with a High-Temperature Furnace," Masters Thesis, Montana State University, August 1967.

31. R. Woodriff and J. Ramelow, Spectrochim. Acta 23B, 665 (1968).

32. R. Woodriff, R. W. Stone, and A. M. Held, Applied Spectrosc. 22, 408 (1968).

33. R. Woodriff and R. W. Stone, Applied Optics, 7, 1337 (1968).

34. R. Woodriff, B. R. Culver, and K. W. Olson, Applied Spectrosc., 24, 530 (1970).

35. R. Woodriff, Abstracts, Society for Applied Spectrosc., New Orleans, LA, No. 207, Oct. 1970.

36. R. Woodriff and D. Shrader, Anal. Chem., 43, 1918 (1971).

37. G. K. Pagenkopf, D. R. Neuman, and R. Woodriff, Anal. Chem., 44, 2248 (1972).

38. R. Woodiff and J. Leck, Anal. Chem., 44, 1323 (1972).

39. J. F. Lech, D. D. Siemer and R. Woodriff, Spectrochim. Acta, 28B, 435 (1973).

40. R. Woodriff, B. R. Culver, D. Shrader and A. B. Super, Anal. Chem., 45, 230 (1973).

41. D. D. Siemer, Applied Spectrosc., 29, 240 (1975).

42. R. Woodriff, Applied Spectrosc., 28, 413 (1974).

43. R. Woodriff, J. R. Amend, D. A. Bath, Abstracts, American Society for testing and materials, Montreal, Canada, June 1975.

44. D. A. Bath, J. R. Amend, and R. Woodriff, Anal. Chem., 50, 1597 (1978).

45. H. Howell, "Effects of Atomization Chamber Size on Constant Temperature Furnaces," Masters Thesis, Montana State University, Dec. 1978.

46. R. Woodriff, J. R. Amend, presentation at Federation of Anal. Chemistry and Spectrosc. Societies, Philadelphia, Penn., 1976.

47. R. Woodriff, M. Marinkovic and R. A. Howald, Anal. Chem. 49, 2008 (1977).

48. M. Marinkovic and R. Woodriff, presenttion at Federation of Anal. Chemistry and Spectrosc. Societies, Philadelphia, Penn., 1976.

49. M. Marinkovic and R. Woodriff, Applied Spectrosc., 30, 458 (1976).

50. F. G. Dewalt, "Construction and Operation of a Woodriff Furnace Atomizer for Atomic Absorption," Honors Thesis, Montana State University, June 1977.

51. M. Marinkovic, R. Woodriff, and I. Eliezer, Spectrochimica Acta, 33B, 765 (1978).

52. J. A. Nichols, R. D. Jones, and R. Woodriff, Anal. Chem., 50, 2071 (1978).

53. J. A. Nichols and R. Woodriff, Anal. Chem., 63, 500 (1980).

54. F. G. Dewalt, J. R. Amend, and R. Woodriff, Applied Spectrosc., 35, 176 (1981).

55. D. D. Siemer, Applied Spectrsc., 32, 245 (1978).

56. T. H. Donnelly, A. J. Eicleston, and R. L. Gally, Applied Spectrosc., 29, 149 (1975).

57. D. D. Siemer, R. Woodriff, and J. Robinson, Applied Spectrosc. 31, 168 (1977).

58. H. Koizumi and K. Yasuda, Anal. Chem., 49, 1679 (1975).

59. H. Koizumi and K. Yasuda, Anal. Chem., 48, 1178, (1976).

60. H. Koizumi and K. Yasuda, Spectrochim. Acta, 31B, 237 (1976).

61. H. Koizumi and K. Yasuda, Spectrochim. Acta, 31B, 523 (1976).

62. H. Koizumi, K. Yasuda and M. Katayama, Anal. Chem. 49 1106 (1977).

63. W. Snelleman, Spectrochim. Acta, 23B, 403 (1968).

64. W. Snelleman, T. C. Rains, K. W. Yee, H. D. Cook and O. Menis, Anal. Chem., 42, 394 (1970).

65. M. S. Epstein and T. C. O'Haver, Spectrochim. Acta, 30B, 135 (1975).

66. G. M. Hieftje and R. J. Sydor, Applied Spectrosc., 26, 624 (1972).

67. R. W. Spillman and H. V. Malmstadt, Anal. Chem. 48, 303 (1976).

68. R. J. Sydor and G. M. Hieftje, Anal. Chem. 48, 535 (1976).

69. R. L. Sellers, G. W. Lowry and R. W. Kane, Am Lab., 5, 61, Mar. (1973).

70. D. W. Brinkman and R. D. Sacks, Anal. Chem., 47, 1723 (1975).

71. R. Woodriff and D. Shrader, Applied Spectrosc. 27, 181, (1973).

72. S. R. Kortyahann and E. E. Pickett, Anal. Chem., 37, 601 (1965).

73. S. R. Koirtyahann and E. E. Pickett, Anal. Chem. 28, 585 (1965).

74. J. Amend, "An Integrating Three-Phase Background Corrected Data Acquisition System for Atomic Absorption Spectroscopy," Proceedings of the Stanford Workshop on Diagnostics for Combustion MHD (1977).

75. J. Amend, "A Three-Phase Background Correcting Data Acquistion System for Atomic Absorption Spectroscopy," MHD Power Generation: Research, Development and Engineering, 1, Annual Report, Oct. (1977).

76. F. G. Dewalt, J. Amend and R. Woodriff, Appl. Spectrosc., 33, 460 (1979).

77. S. R. Lawson, F. G. Dewalt and R. Woodriff, Progress in Analytical Atomic Spectroscopy, in press.

78. W. Frech and A. Cedergen, Anal. Chim. Acta 82, 83 (1976).

79. E. L. Wheeler, Scientific Glassblowing, Interscience Publishers, Inc., New York, (1958).

MONTANA STATE UNIVERSITY LIBRARIES
stks D378.D512@Theses RL
Design, operation and optimization of an
3 1762 00177746 3

D378
D512
cop 2